HEALTH MONITORING OF PRECAST BRIDGE DECK PANELS REINFORCED WITH GLASS FIBER REINFORCED POLYMER BARS

by

James McDaniel Ries

A thesis submitted to the faculty of
The University of Utah
in partial fulfillment of the requirements for the degree of

Master of Science

Department of Civil and Environmental Engineering

The University of Utah

May 2011

The University of Utah Graduate School

STATEMENT OF THESIS APPROVAL

The thesis of **James McDaniel Ries**

has been approved by the following supervisory committee members:

Chris Pantelides	, Chair	**4/19/2011** Date Approved
Lawrence Reaveley	, Member	**4/19/2011** Date Approved
Paul Tikalsky	, Member	**4/19/2011** Date Approved

and by **Paul Tikalsky** , Chair of

the Department of **Civil and Environmental Engineering**

and by Charles A. Wight, Dean of The Graduate School.

ABSTRACT

The Beaver Creek Bridge on US highway 6 is the pilot project for Glass Fiber Reinforced Polymer (GFRP) bridge decks and posttensioned bridge decks in the state of Utah. The bridge was built in 2009, using accelerated bridge construction practices, including the use of precast prestressed girders, as well as precast decking. The west-bound bridge decking was composed of 12 precast panels each measuring 41'-5" long, 6'-10" wide, and 9¼" thick, and weighing approximately 33 kips. At the time, these panels were the longest GFRP panels in the United States.

The Utah Department of Transportation has decided to evaluate GFRP reinforcing bars as an alternative to steel rebar in this bridge deck. The hope is to increase the lifespan of bridge decks to match the service life of the entire bridge. Due to the nature of the GFRP bars, the panels were lifted at four points using straps instead of imbedded anchors. During the four-point lifting, the panels exhibited small deflections and strains; furthermore, no cracks larger than hairline cracks were found in the panels after lifting.

The Beaver Creek Bridge deck is the first precast deck in the state of Utah to be posttensioned in the direction of traffic. Posttensioning bridge decks is expected to become the norm in the state of Utah. The posttensioning resulted in increased continuity between panels.

In order to quantify the expected performance of the bridge during its service life, a truck load test was performed. The truck load test was comprised of a static and

dynamic test. During the truck load test, the bridge experienced deflections in the panels which were 93% below design values. Girder deflections were also small.

The use of GFRP bars has the potential to extend the life of bridge decks exposed to deicing salts from 45 years to 100 years, while only requiring an increased capital cost in the bridge of 8%. Furthermore, the use of GFRP bars in conjunction with accelerated building practices has the potential to reduce long-term user delays resulting from maintenance. The difference in capital cost could decrease as designers become more comfortable with the material and gain experience with the system.

TABLE OF CONTENTS

LIST OF TABLES

LIST OF SYMBOLS AND ABBREVIATIONS

GFRP	=	Glass fiber reinforced polymer
LVDT	=	Linear variable differential transformer
TLT	=	Truck load test
VWSG	=	Vibrating wire strain gauge
EP3	=	End panel three
P2-05	=	Phase two panel five
ACI	=	American concrete institute
PCI	=	Precast cast institute
E_c	=	Modulus of elasticity of concrete
I	=	Gross moment of inertia
I_e	=	Effective moment of inertia
φ	=	Curvature
ε	=	Strain
d	=	Distance between the top and bottom reinforcing mats
M_t	=	Theoretical moment
M_{LL}	=	Moment from design live load
l_{eff}	=	Effective distance between girders
RC	=	Reinforced concrete

ACKNOWLEDGEMENTS

I, James Ries, the author of this paper, would like to acknowledge the contributions of Dr. Pantelides, without whom this project would not have been possible. His patience and diligence got us through this project. Additionally, this thesis was made possible through the near constant support of Emily Dages. I would like to thank Brandon Besser and Ruifin Liu, who aided in the attachment of foil gauges to the GFRP bars. I would like to thank Michael Adams, who taught me how to use the vast amount of hardware and software involved with this project. I would like to thank my parents, first, for bringing me into this world, and second, for raising me to have the determination to finish this project. I would also like to thank the multiple construction crews who went out of their way multiple times to accommodate this project. Special thanks to Clayton Birmingham and Brett Raddon for helping out with the truckload test, and Rebecca Nix for providing us with so much of the background information regarding the bridge and the overall process.

CHAPTER 1

INTRODUCTION

1.1 Project Introduction

In recent years, the Utah Department of Transportation (UDOT) has taken progressive measures to increase the lifespan of its bridges as well as to decrease user delays. These measures include the use of accelerated bridge construction practices and the exploration of materials which decrease scheduled maintenance resulting from corrosion. UDOT decided to evaluate Glass Fiber Reinforced Polymer (GFRP) reinforcing bars as an alternative to steel rebar in bridge decks, to determine if its use would increase the lifespan of bridge decks to match the service life of the entire bridge.

During the summer of 2009, construction began on the Beaver Creek Bridge, located approximately 20 miles north of Price Utah on US-6, as seen in Figure 1. The Beaver Creek Bridge deck was constructed using GFRP bars instead of traditional steel reinforcing bars. GFRP bars offer many advantages over traditional steel reinforcing bars, including increased tensile strength, decreased unit weight, and corrosion resistance. Using GFRP bars in a bridge deck has been hypothesized to extend the life of the bridge deck up to 100 years (Benmokrane et al. 2006).

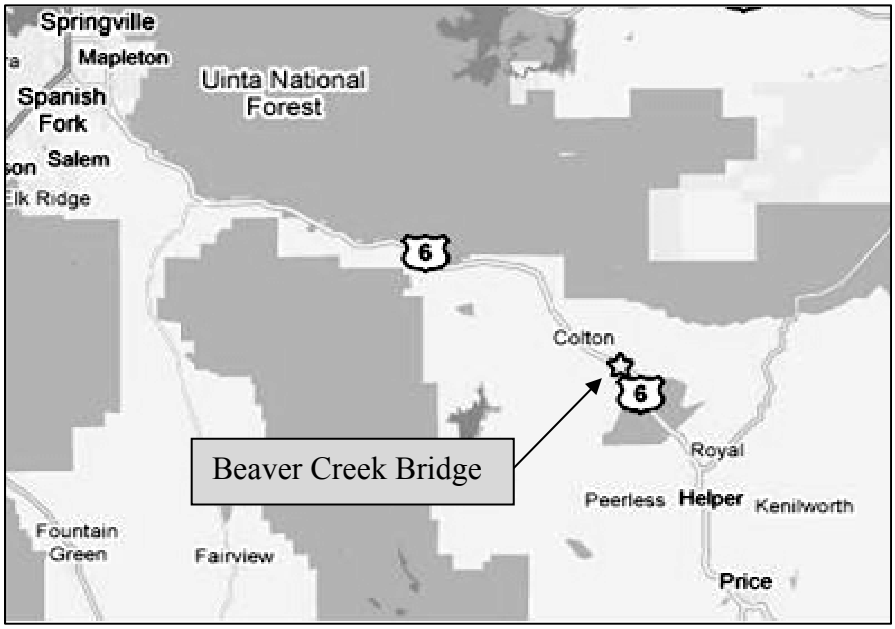

Figure 1. Location of bridge on US-6

The Beaver Creek Bridge is a single-span creek crossing with access for wildlife passage. The bridge is composed of twelve AASHTO Type IV prestressed girders (AASHTO 2009) running the span of the bridge with two sets of panels lying perpendicularly atop the girders, twelve for each direction of traffic. The bridge has an overall span length of 88'-2" and an out to out width of 88'-10", as shown in Figure 2. The deck was designed in accordance with ACI 440.1 R-06 (2006), and constructed using 24 precast deck panels. The bridge was constructed in two phases, each focusing on a different direction of traffic. Phase one constructed the east-bound direction, and was composed of twelve precast panels measuring 44'-5" long, 6'-10" wide, and 9¼" thick. Phase two constructed the west-bound bridge; its decking was composed of 12 similar panels each measuring 41'-5" long, 6'-10" wide, and 9¼" thick, and weighing approximately 33 kips, as seen in Figure 3, Figure 4, and Figure 5. This project focuses on phase two of the Beaver Creek Bridge project.

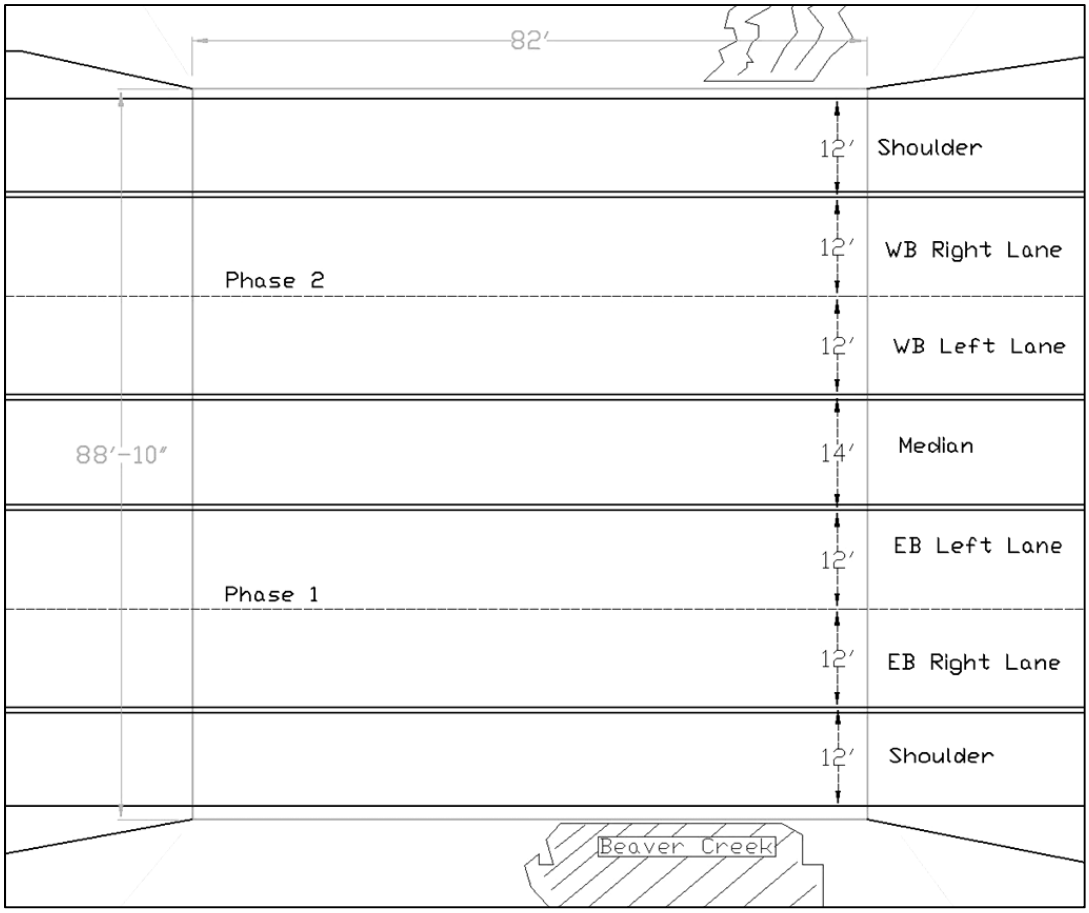

Figure 2. Plan of bridge

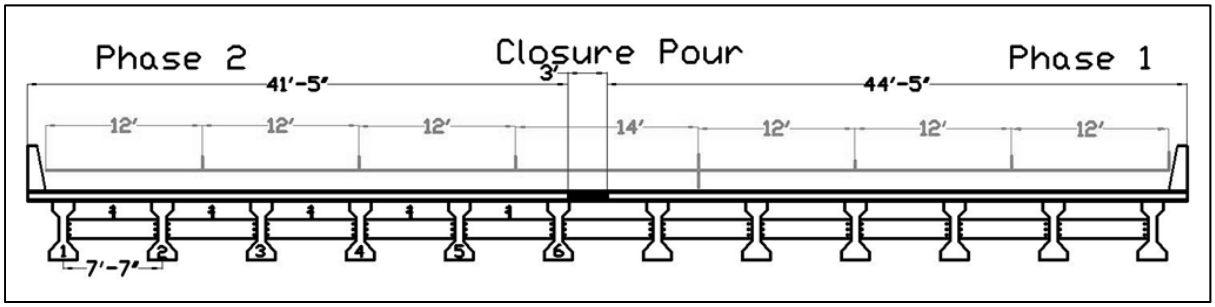

Figure 3. Bridge cross section looking east

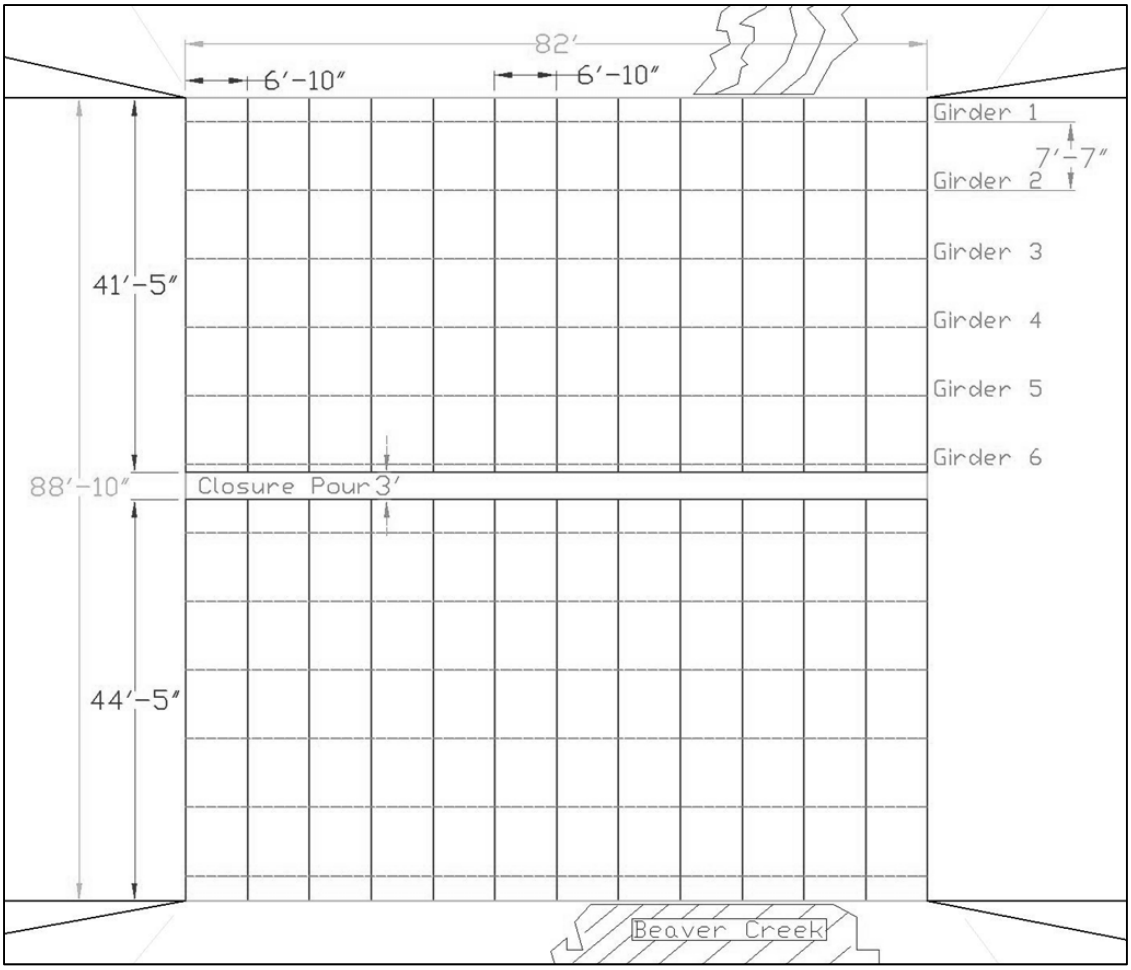

Figure 4. Bridge plan showing panels and girders

Figure 5. Panel EP3 sitting in the precast yard with approach slab rebar on the right

The twenty-four deck panels were fabricated in Pleasant Grove Utah, individually transported 64 miles to the bridge site, and lifted into place. Each of the panels were lifted a total of three times before ending up in their service position. The first lift removed the deck panel from its formwork. This lift took place before the parapet had been cast. Once the parapets had been cast, a second lift placed the panel on the bed of a tractor trailer. The final lift placed the panel atop the girders.

Once the panels were in place, they were vertically adjusted using leveling bolts. Once adjusted, the panels were fastened to the girders using bolts in the sheer stud blockouts to increase the composite action with the girders, as seen in Figure 6. Afterwards, the sheer stud blockouts and vertical adjustment bolts were filled with nonshrink grout. Finally, a closure pour connected the two sets of panels providing continuity to the panels, as seen in Figure 3.

The deck panels were partially posttensioned in the direction of traffic flow, to increase the shear transfer of the grout key between the panels, and to reduce the potential for cracking. Here the word “partially” refers to the intensity at which the posttensioning strands where tensioned. Typically posttensioning strands of this size have a jacking force of 46.9 kips applied to them; however, the tendons in this application were only jacked to 40.8 kips.

1.2 Literature Review

There has been much work done in the area of GFRP reinforced bridge decks and truck load tests. Benmokrane et al. (2006) describes a project similar in nature to the

Figure 6. Leveling bolts and shear stud blockouts.

Beaver Creek Bridge project; the paper is concerned with the Morristown Bridge on Route 100 in Morristown Vermont. At the time, the Morristown Bridge was the first bridge in the world of its size and category fully reinforced with GFRP bars. Crack width was the controlling design factor and determined the bar size and spacing. The maximum design crack width was 0.019 in. Benmokrane offers a good overview of the need for GFRP bars in North America given the freeze thaw cycles and use of deicing salts. The paper also overviews the methodology of live load testing for bridges. Benmokrane monitored strain in the bridge deck using fiber optic sensors, and monitored the midspan girder deflections using a system of rulers and a theodolite. Strains in the GFRP bars recorded during the live load test were less than 0.2% of the ultimate strain. The paper suggests that the AASHTO flexural design method overestimates the calculated design moments for both service and ultimate.

Another project, similar to the present one, is detailed in the dissertation of Eitel (2005). This project involves a bridge in Ohio where the steel reinforced deck was replaced with one using GFRP bars. At the time, this project represented the first utilization of entirely GFRP nontensioned reinforcement in a deck on a multispan vehicular bridge worldwide. The author describes in detail the chemical process where steel oxidizes and the resultant degradation to infrastructure. The goal of the project was to collect strain, temperature, and deflection data from the bridge through seasonal changes. In the project, the researchers instrumented foil strain gauges on the GFRP bars as well as on the surface of the concrete. The deflection data were measured using linear variable differential transducers (LVDT) placed in the middle of the diaphragms. This paper offers results from six slow moving truck load tests, during which the maximum strain in the bars never exceeded 0.3% of the guaranteed tensile strength. The rehabilitated deck was found to have enhanced stiffness as well as greater continuity.

Eitel referred to a study in which GFRP bars were found to have degraded stiffness and strength as a result of prolonged direct exposure to alkaline solutions. An accelerated ageing investigation of the Aslan™ 100 bars was conducted in a 13PH calcium hydroxide solution at 176 degrees Fahrenheit for 28 days to simulate 50 years of service life. The investigation showed 16% degradation in tensile strength and 4% degradation in modulus of elasticity. However, there were problems with the test methodology and the aging process was found to have been too harsh. These finding have led to conservatism in design, whereas degradations were accounted for; this work has since been refuted.

More recent work done involving the ISIS network in Canada (Mufti 2007) has found that there was no degradation in bars removed from service after 5-8 years. In 2004, an extensive study was conducted across Canada, wherein concrete cores were removed from GFRP bridge decks after being in service for 5-8 years. The decks had been exposed to wet-dry cycles, marine environments, freeze-thaw cycles, and deicing salts. The samples were tested using a number of methods, including optical microscopy and scanning electron microscopy. The chemical matrix of the GFRP bars was examined for changes using Fourier Transformed Infrared Spectroscopy, and no changes in, or hydration of, the matrix were found. Overall, the researcher found that "GFRP is durable in concrete" (Mufti 2007).

Another bridge instrumentation project was detailed by (Camisa et al. 2003), and involves the instrumentation of a multispan section of the SR 56 Kernville Viaduct in Pennsylvania. The project aimed to gather strain and temperature data from imbedded vibrating wire strain gauges and thermistors. Using the data, they hoped to assess the performance of the deck. Gauges were placed at 5 locations across the three spans, including four locations at the points of maximum positive and negative moment, as well as one location at the point of contraflexure. Data from the VWSGs were collected using a data logger and periodically downloaded to an onsite laptop. No results were reported.

Recent work done by Weber and Baquero (2010) has resulted in a new durability concept for GFRP bars, which has been accepted and adopted by *The International Federation for Structural Concrete*, also called "fib." The previous measure of durability focuses on a residual strength approach, wherein the bars are allowed to age in an alkaline solution under no load, or very small load, then tested for strength. The new

approach takes into consideration environmental conditions such as humidity, mean temperature, and amplitude of temperature fluctuations; furthermore, it ages the bars in realistic conditions, embedded in concrete saturated with an alkaline solution, and under a wide variety of constant stresses. The new concept treats tensile strength, alkali resistance, and creep rupture integrally, and measures the interactions among them; furthermore, it is independent of bar diameter. During the project, bars were tested in accordance with ACI 440.3R-04R at elevated temperatures, and under a wide range of stress levels. The authors observed two dramatic trends during the project:

> Tests showed that below a threshold stress level, the residual strength is essentially independent of the stress applied on the bars during the aging process- remaining at about 90% of the virgin strength. When the bars are aged at stresses above the threshold, however, they fail suddenly before their residual strength can be tested. In other words their residual strength goes to zero. (Weber and Baquero 2010)

Additional tests at lower stress levels were carried out to determine a time-to-failure line. “The relationship between the applied stress and the time to failure is linear on a log-log plot.” The time-to-failure line was then extrapolated in accordance with the German standard DIN 53768. Additionally, it was observed that the rate of strength reduction for tests performed at 73° and 100° were nearly identical, while tests performed at 140° had an increase in the rate of strength reduction. The authors provided a table of generalized applications corresponding to environmental conditions, member thicknesses, effective temperatures, and design service life. For a 6 in. thick bridge deck exposed to outdoor conditions, with an effective temperature of 77°, the authors recommend a design service life of 100 years (Weber and Baquero 2010).

1.4 Overview of Glass Fiber Reinforced Polymers Bars

Glass Fiber Reinforced Polymer bars are a substitute for traditional steel reinforcing, and at the most basic level, the material is similar to the fiberglass used widely today. GFRP bars are made from long strands of high strength E-glass (alumino-borosilicate). The strands are bound together with S-glass (alumino silicate). The two glasses and a few additives and fillers are combined with a vinyl ester resin in a pultrusion process to create the bars seen in Figure 7. This process is combined with an in-line coating process to obtain exterior adhesion properties (Tang 1997).

Glass Fiber Reinforced Polymer bars offer many advantages over traditional steel reinforcement. The first is corrosion resistance: GFRP bars will not oxidize or change their chemical makeup; they are impervious to the action of salt ions and the alkalinity inherent in concrete. Corrosion resistance is the biggest factor in reducing long-term costs of bridge decks; it is also the primary reason GFRP bars are chosen for a given application.

Figure 7. Close-up of GFRP bar

The second advantage is their weight. GFRP bars are light weight, having a unit weight approximately one-fourth that of steel rebar. This offers increased usability and savings in both handling and placement. GFRP bars are void of any metallic substances and are nonconductive. This means that GFRP bars are electromagnetically neutral and will not interfere with the operation of sensitive electronic devices such as medical MRI units or electronic testing devices. Lastly, GFRP bars do not conduct heat in the same way as steel rebar does, making them a thermal insulator by comparison (Tang 1997).

GFRP bars do, however, have a few disadvantages when compared with traditional steel reinforcing bars. GFRP bars are more expensive than traditional steel reinforcement. However, their applications are very specialized. Using GFRP bars in a bridge deck may only increase the cost of the bridge by approximately 4% (Benmokrane et al. 2006). For comparison, the cost for using GFRP bars for the Beaver Creek Bridge increased the total cost of the bridge by 8% (Rebecca Nix, personal communication, January, 2011).

The second disadvantage of GFRP bars is its low modulus of elasticity. Finished GFRP bars have a modulus of elasticity of approximately 5,920 Ksi, about one-fifth that of steel. The lower modulus means that slabs and structures built with GFRP will have higher deflection. For deflection limit-based design, the number of bars in a given structure will most likely have to be increased to maintain the same deflections as those with steel reinforcing (Hughes Bros 2009).

The final disadvantage of GFRP bars is their inability to be altered in the field. GFRP bars cannot be bent after they have been cured and since they are shipped in a fully-cured form, they cannot be bent onsite. Bends can, however, be produced during the

manufacturing process in virtually any shape that can be obtained with steel rebar; however, a more generous bend diameter is required. Furthermore, planning for all bends will have to be taken into consideration ahead of construction, and change orders involving GFRP bars are typically more expensive that those involving steel (Hughes Bros 2009).

1.5 Material Properties of GFRP Bars

The properties of the GFRP bars used in the Beaver Creek Bridge were provided by the manufacturer and are summarized in Table 1 (Hughes Bros 2009). Table 2 offers a comparison of typical properties for two common bars. From the table, we can see the weight and tensile strength advantages of GFRP bars at the fundamental level. We can also see the advantage steel has over GFRP bars in its elastic modulus.

Table 1 Material properties of GFRP bars used in Beaver Creek Bridge

Guaranteed ultimate tensile strength	95,000 psi
Tensile strength average	120,396 psi
Modulus of elasticity	7,190,000 psi
Ultimate strain	0.0167 in./in.

Table 2. Comparison between Aslan 100 GFRP and grade 60 steel

	Units	Aslan 100 GFRP (#5)	Grade 60 Steel
Ult. tensile strength	Ksi	95	80
Modulus of elasticity	x 10^3 Ksi	5.92	29
Specific gravity	Unitless	2.0	7.85
Strain at failure	%	1.7	6-12
Thermal conductivity	Btu-in/(ft^2 hr F)	~5	360

In compression, GFRP bars have been found to have approximately half their tensile strength, while maintaining their modulus of elasticity. In compression, three failure modes are possible: crushing, buckling, and combined buckling and crushing. The crushing mode represents the failure mode a GFRP rebar would experience when confined in concrete under compression. Young's modulus of GFRP bars in compression is approximately the same as in tension, although the testing was limited (Deitz et al. 2003).

1.6 Design of Bridge and Changes in Design to Accommodate GFRP

The design of the deck panels was controlled by crack width and deflection. The low modulus of elasticity of GFRP bars may lead to wider crack widths than with traditional steel. The acceptable crack width tolerances can be relaxed some with GFRP bars due to their noncorrosive nature. However, the wider crack widths can lead to loss of aggregate interlock and a reduction in shear capacity. GFRP reinforcement also exhibits higher deflections than steel. Due to these design limitations, several adjustments had to be made to the structural design. The first adjustment was to the bar spacing; in the transverse direction, the spacing was reduced from 8 in. (203mm) down to 4 in. (102mm) effectively doubling the numbers of bars. This adjustment was the direct result of the low modulus of elasticity of the GFRP bars, and based on deflection calculations.

It was not economical to reduce the spacing any further, so alternative methods for decreasing crack width and deflection had to be used. A balance between thickening the deck and decreasing girder spacing was used. The deck was increased from the standard 8½ in. (216mm) thickness, up to 9¼ in. (235mm). The girder spacing was

decreased from 9 ft-4 in. (2.845m), down to 7 ft-7 in. (2.311m), increasing the number of girders by two (Rebecca Nix, personal communication, October, 2010).

The GFRP reinforcing posed some additional challenges. Traditional deck panels are lifted and positioned using embedded anchors. However, due to the low shear capacity of the GFRP bars, the panels had to be lifted using straps which wrapped around the panel and supporting them from below, making the positioning process awkward, time consuming, and difficult (Rebecca Nix, personal communication, October, 2010).

Moreover, the GFRP bars could not provide enough shear strength for the posttensioning anchors. To compensate, some supplementary steel reinforcing was used on the end panels to provide additional strength to the posttensioning anchors and aid in stress distribution, as seen in Figure 8. Additionally, extra GFRP bars were used to reinforce the area around the posttensioning anchors (Rebecca Nix, personal communication, October, 2010).

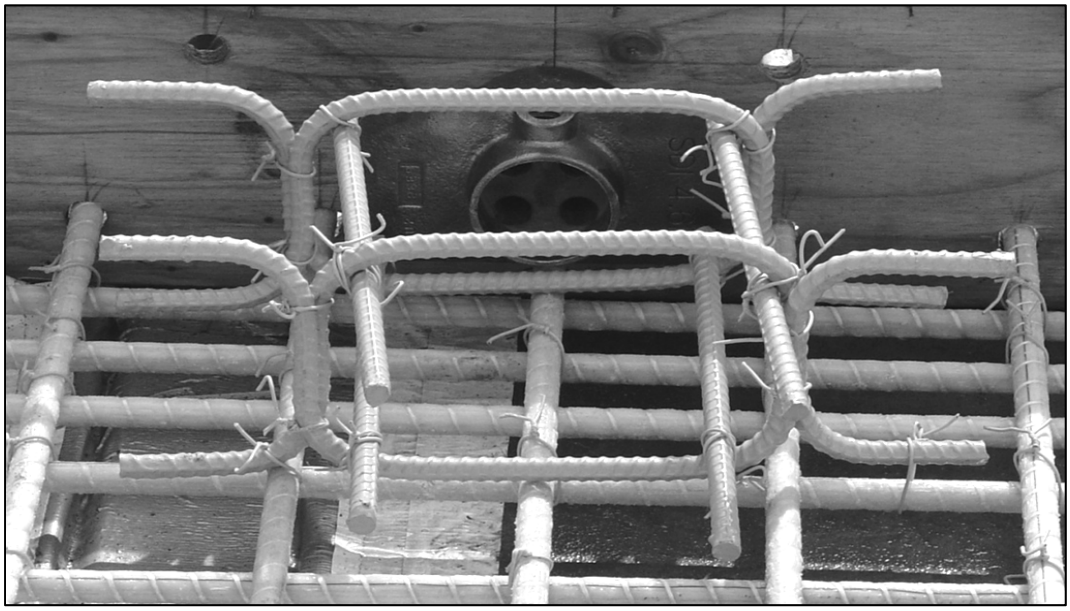

Figure 8. Steel reinforcing to accommodate increased shear demanded from posttensioning anchor

The reinforcement consisted of #5 (Φ16mm) GFRP bars spaced every 4 in. in both the transverse and longitudinal directions and in both the top and bottom mats. The concrete used for the precast concrete panels had a 28-day compressive strength of 6,200 psi (43 MPa).

The bridge design live load used the AASHTO HL-93 design vehicle. This loading is the combination of either a design tandem (two axles, 25 kips/axle, spaced 4 ft. apart) or the HS20-44 design truck with a distributed lane load of 0.64 kips/foot. By comparison, this load is larger and more concentrated than the load seen during the truck load test.

CHAPTER 2

EXPERIMENTAL DESIGN

2.1 Scope

This project attempted to accomplish a number of goals related to health monitoring of the Beaver Creek Bridge. They can be separated into two categories: construction goals to be accomplished during the construction phase, and postconstruction goals to be accomplished once construction had concluded. The goals include:

1. Instrument two deck panels associated with phase two of the Beaver Creek Bridge. Obtain and report data in real time during the three panel lifts, as well as during transportation. Instrument the Beaver Creek bridge girders and diaphragms with sensors. Instrument the bridge site with a still camera, atmospheric sensor, and antenna. Setup the data loggers for automatic data acquisition.
2. Monitor the two panels during every move from initial casting to final placement. Strain data were taken using embedded foil strain gauges attached directly to the GFRP reinforcing.
3. Compare the measured curvature diagram from lifting provided by the foil strain gauges with those extrapolated from the PCI handbook by taking the predicted moment provided by PCI and calculating the theoretical curvature diagram.

4. Record strains during the posttensioning process using the vibrating wire strain gauges. Compare the theoretical posttensioning strains with those recorded from the sensors.
5. Perform static and dynamic truck load tests in which both west-bound lanes would be tested independently as well as simultaneously. The truck load test gathered girder deflections at midspan, panel deflections between girders, peak vertical accelerations of girders at midspan, and internal strains.
6. Determine if the changes made to the design of the bridge to accommodate GFRP bars were successful in preventing the deck from cracking and maintaining small service deflections.
7. Determine if a trend exists within the accelerometer data relating velocity to maximum acceleration.
8. Compare the cost of the GFRP deck to a traditional reinforced concrete steel deck. Analysis will be conducted on a per year basis, and include the extraneous costs of using GFRP.

2.2 Experimental Setup

Due to the decreased modulus of the GFRP bars, the deck had to be lifted using straps instead of embedded anchors. For each lift, the panels where lifted at four points. Strap locations are shown in Figure 9 and Figure 10 .

The truck load test (TLT) consists of nine static tests and six dynamics tests, all preformed on the west-bound direction of traffic. Tests 1-3 were preformed on the right lane using truck “A”. Tests 4-6 were preformed on the left lane using truck “B”.

Figure 9. Panel P2-05 being lifted using straps at the bridge site

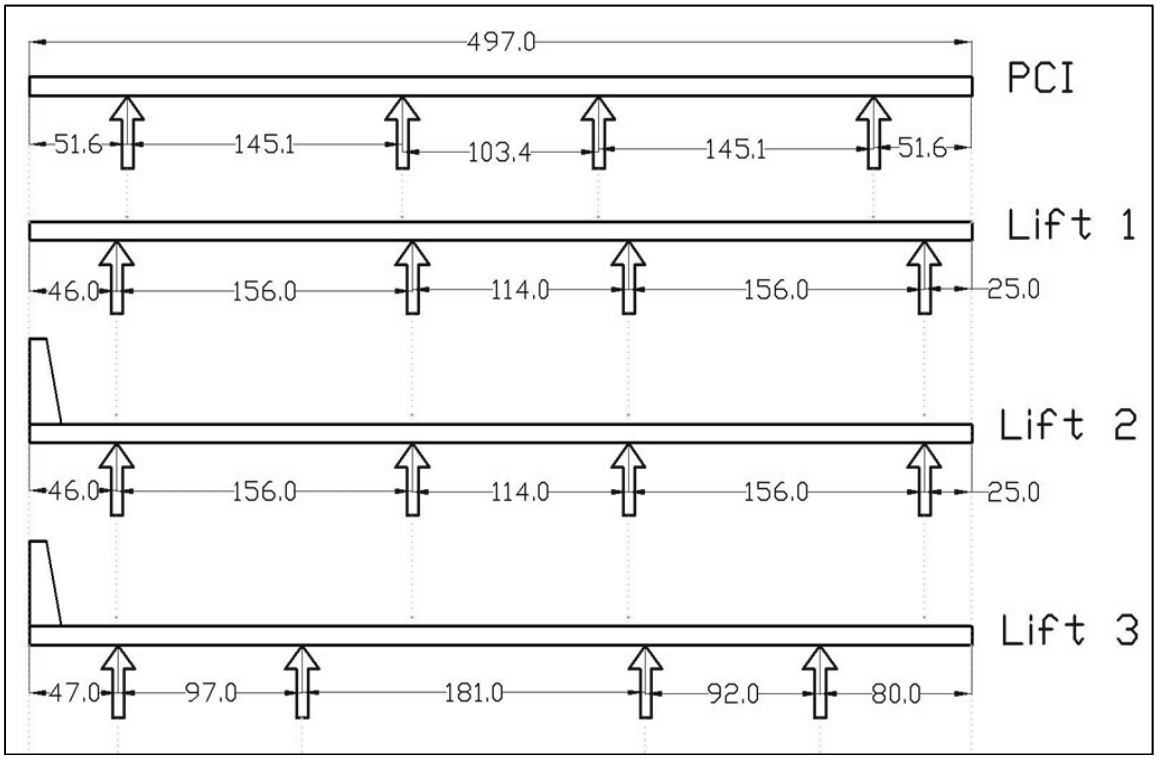

Figure 10. Lifting point diagram (all dimensions in inches)

combination of tests 1-3 and 4-6, respectively, and used both trucks in their respective lanes. Table 3 provides details on the trucks “A” and “B” as well as some details about the HL-93 design vehicle. Figure 11 provides dimensions for the two test trucks. Table 4 provides an overview of the static tests performed. Figure 12 provides details about each of the tests. Three types of data were taken for each of the static truck load test, including midspan girder deflections, panel deflections relative to the girders, and concrete strains in both transverse and longitudinal direction.

Table 3. Truck weights

	Axle weight (lbs.)		
	Truck A	Truck B	HL-93 design truck
Front axle	14,780	14,480	8,000
1st Rear axle	14,550	14,340	32,000
2nd Rear axle	14,550	14,340	32,000
Gross WT.	43,880	43,160	72,000

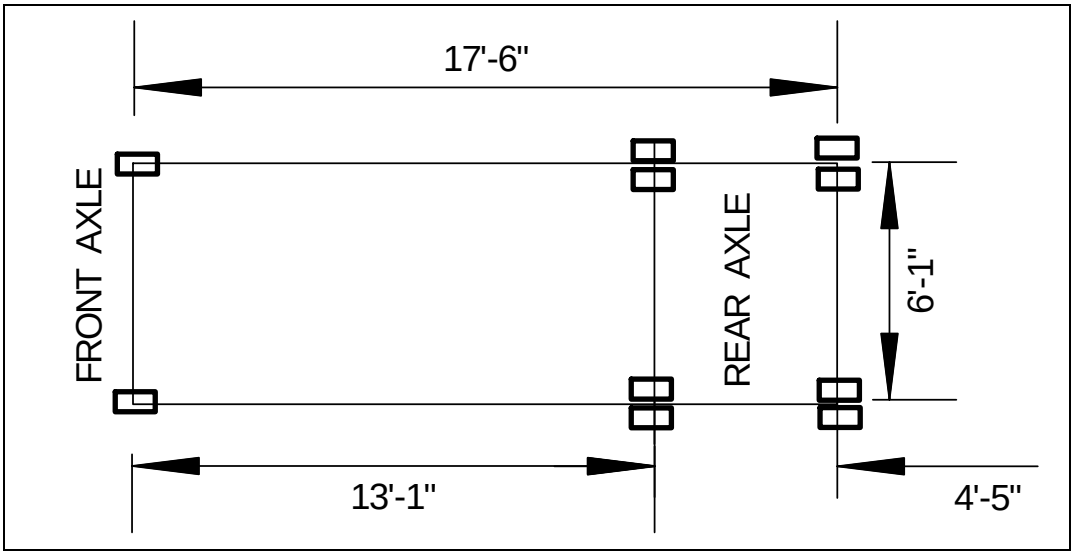

Figure 11. Test truck dimensions

Table 4. Static test positions

Test #	Type of test	Lane tested	Truck used	Rear axle position
1	Static	Right	A	East Diaphragm
2	Static	Right	A	Midspan
3	Static	Right	A	West Diaphragm
4	Static	Left	B	East Diaphragm
5	Static	Left	B	Midspan
6	Static	Left	B	West Diaphragm
7	Static	Both	A&B	East Diaphragm
8	Static	Both	A&B	Midspan
9	Static	Both	A&B	West Diaphragm

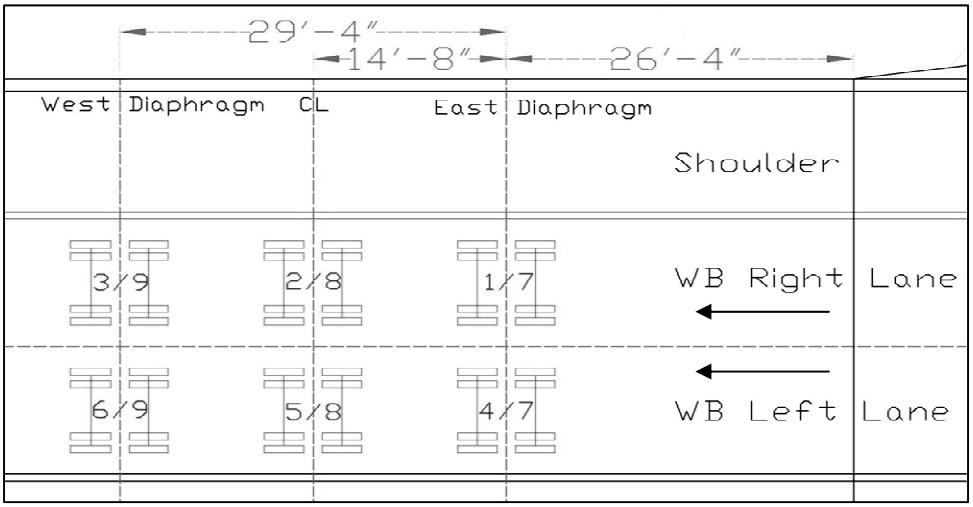

Figure 12. Locations of trucks during truck load test

Truck load tests 10 through 15 were dynamic tests, with trucks “A” and “B” driving westward across the west-bound direction of the bridge. Test 10 and 11 were conducted at 40 mph with each truck in its respective lane. Test 12 was performed with both trucks simultaneously traveling at a speed of 35 mph. Test 13 and 14 were faster versions of test 10 and 11 and were conducted at 65 mph. Test 15 was not conducted due to safety concerns about the length of runoff area for the truck. The dynamic truck load tests are summarized in Table 5.

Table 5. Dynamic test details

Test #	Type of test	lane tested	Truck used	Velocity (mph)
10	Dynamic	Right	A	40
11	Dynamic	Left	B	40
12	Dynamic	Both	A&B	35
13	Dynamic	Right	A	65
14	Dynamic	Left	B	65
15	Dynamic	Both	A&B	Not performed

2.3 Instrumentation Setup

Two panels were chosen for instrumentation due to their location on the bridge: "End Panel Three" (EP3) is located toward the west end of the bridge and "Phase Two Panel Five" (P2-05) is located at the midspan of the bridge, as seen in Figure 13.

This project used two types of strain gauges for monitoring the strains inside the panels. It also used displacement sensors for monitoring the performance of the panel, and accelerometers to monitor peak accelerations of the bridge girders at midspan. Furthermore, one sensor was used to monitor the atmospheric conditions at the bridge site. In addition to the five sensors mentioned above, surveying equipment was employed to determine the midspan deflection of the girders.

2.3.1 Foil Gauges

Each panel was instrumented with twenty-eight foil strain gauges, to be used during the lifting and transportation of the panels. These gauges were attached directly to both the top and bottom GFRP mats and recorded the strains in the bars. Of the twenty-eight foil gauges, twenty were placed in the transverse direction of the bridge

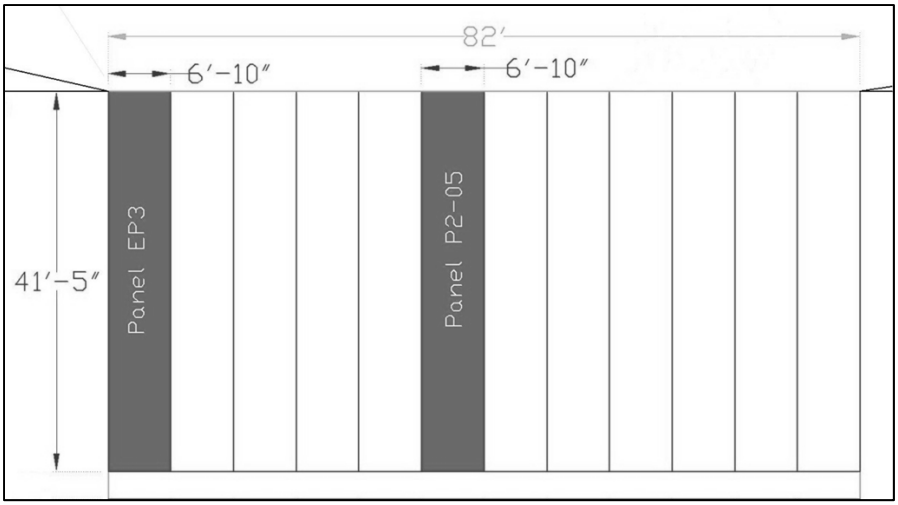

Figure 13. Plan of bridge with instruments and panel

(longitudinal direction of the panel) to record strains in the long direction of the panel during lifting. The remaining eight gauges were placed in the longitudinal direction to record strains in the short direction. Figure 14 provides a more detailed look at the locations of the foil gauges. Gauge locations where chosen due to their proximity to the lifting points and point of maximum theoretical moment. Foil gauges were chosen due to their high sampling rate potential, relatively low cost, and overall simplicity. Their drawbacks include their difficulty in attachment to GFRP bars, as well as their short life span.

2.3.2 Vibrating Wire Strain Gauges

Panels EP3 and P2-05 were each instrumented with four vibrating wire strain gauges (VWSG) placed in the longitudinal direction of the bridge. These gauges were used to record strains in the concrete induced by posttensioning as well as the change in strain due to creep and other long-term effects.

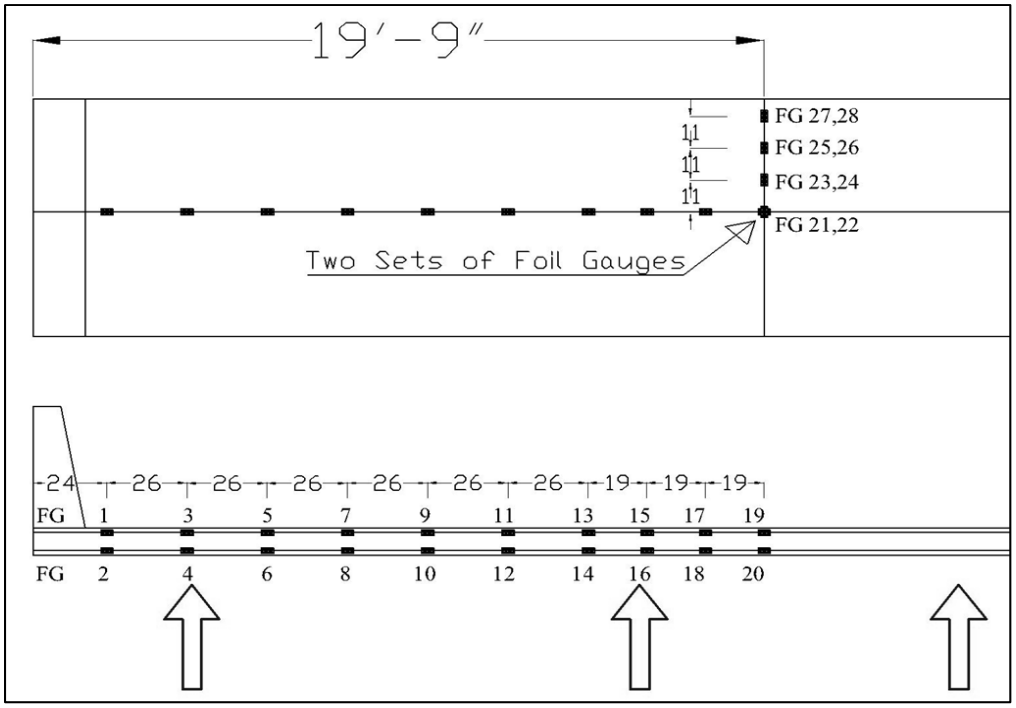

Figure 14. Foil gauge locations for both panels

In addition to the four longitudinal VWSGs, panel P2-05 was equipped with an additional sixteen VWSG placed in the transverse direction of the bridge, as seen in Figure 15. These gauges were primarily used during the truck load test and long-term monitoring. Gauge locations where chosen due to their proximity to the girders and locations of the trucks during the truck load test. The strengths of the VWSGs including a long life span, a built in thermistor, and ease of installation; however, they have a relatively low sampling rate, on the order of two seconds per sensor.

The VWSG were secured to the GFRP mats using zip ties and foam blocks, and lie in the same horizontal plane as the GFRP mats, as seen in Figure 16. Each of the VWSGs has a built in thermistor which records the interior temperature of the panel. The maximum sampling rate for a VWSG is approximately two seconds and the sampling must be done one sensor at a time.

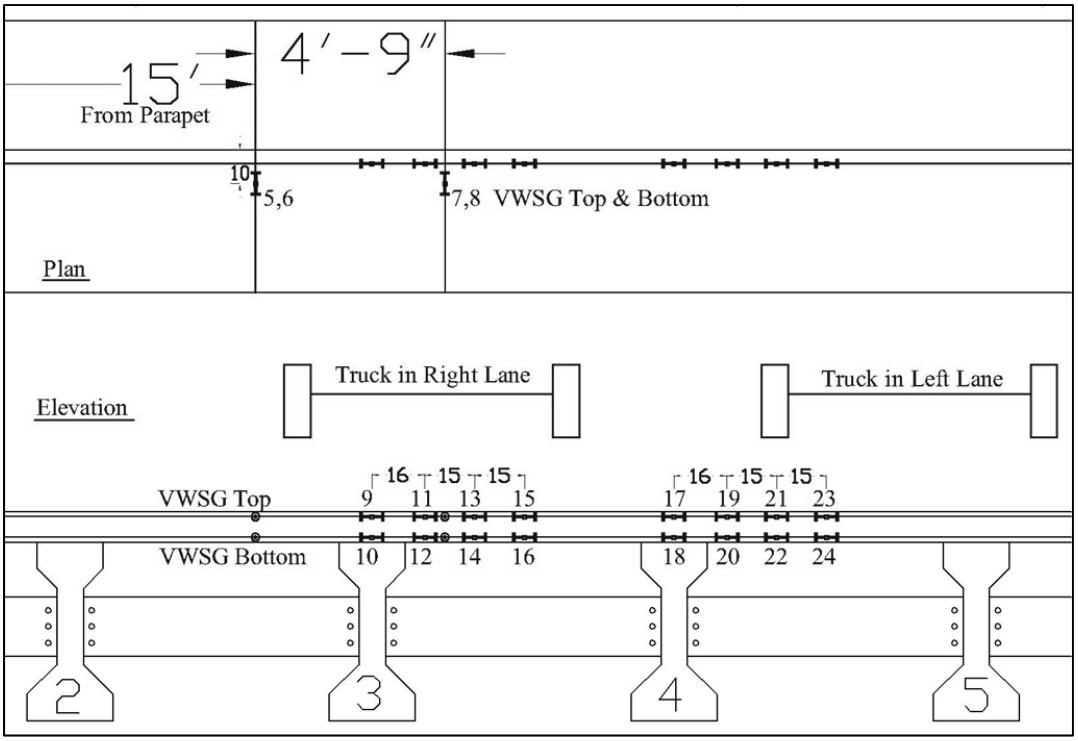

Figure 15. VWSG locations

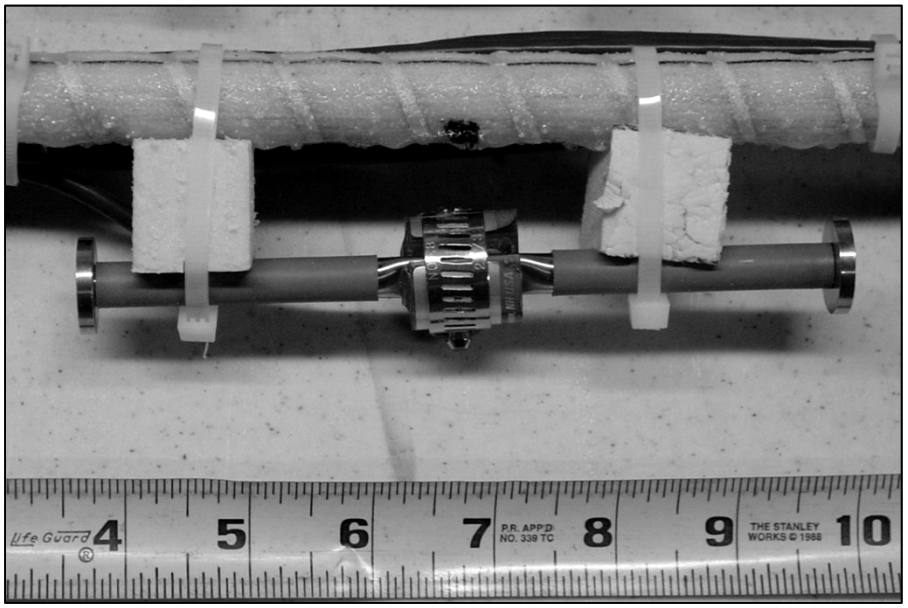

Figure 16. Close up of Vibrating Wire Strain Gauge attached to GFRP rebar with zip ties and foam blocks

2.3.3 Linear Variable Differential Transducer (LVDT)

The bridge was instrumented with six LVDTs. These sensors were placed above the diaphragms midway between the girders, to measure the deflection of the deck relative to the girders. LVDTs #1-#5 were placed above the west diaphragms between girders 1 through 6, respectively. LVDT #6 was placed between the second and third girder above the east diaphragm, directly across from LVDT #2. The LVDTs were attached to the diaphragms using hose clamps and a piece of square bar welded directly to the diaphragm, as seen in Figure 17.

2.3.4 Accelerometers

The bridge was instrumented with six single-axis accelerometers. The accelerometers were attached to the bottoms of girders 1-6 at the midspan of the bridge, with vertical axes of measurement. They were used during the truck load test for peak accelerations, and during long-term monitoring for the collection of acceleration signatures and the triggering of the camera. The accelerometers have a sampling rate of up to 50 hertz and a sensitivity of 0.001g.

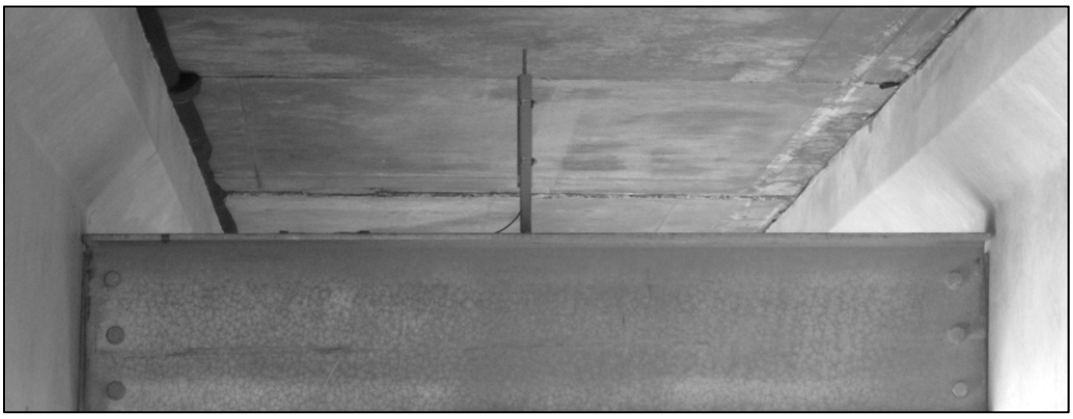

Figure 17. LVDT attached to diaphragm under bridge

2.3.5 Atmospheric

Atmospheric data were collected using an HMP-50 from Campbell Scientific. The sensor was mounted to a fence post adjacent to the bridge, as seen in Figure 18. Data were averaged and recorded every 12 hours. The HMP-50 records both relative humidity as well as temperature. The accuracy of the relative humidity sensor is ±3% (0% to 90% range) and ±5% (90% to 98% range), the temperature sensor has a range of -40° to +60°C and is accurate to within 0.1 degree.

2.3.6 Surveying Equipment

In addition to the five sensors mentioned above, surveying equipment was used to determine the midspan deflection of the six girders for each of the nine static truck load tests. A Sokkia SLD30 power level was operated with a RAB (RAndom Bidirectional) code elevation staff to provide the deflections of the girders. The staff was held against the bottom of the girder by an operator in a JLG lift positioned under the bridge, as seen in Figure 19.

2.3.7 Camera

A still camera was mounted atop a 15 ft. tall post stationed approximately 30 ft. north of the west abutment, as seen in Figure 20 and Figure 21. The camera was aimed toward the bridge with the lens setting on wide, as seen in Figure 22. The purpose of the camera was to obtain a visual record of what caused the largest accelerations. The camera is triggered whenever accelerometer #5 meets a specific threshold, typically around 0.025g.

Figure 18. HMP-50 in its protective housing attached to fence post adjacent to bridge

Figure 19. Surveying team for truck load test

Figure 20. Still camera used for visual record of largest accelerations

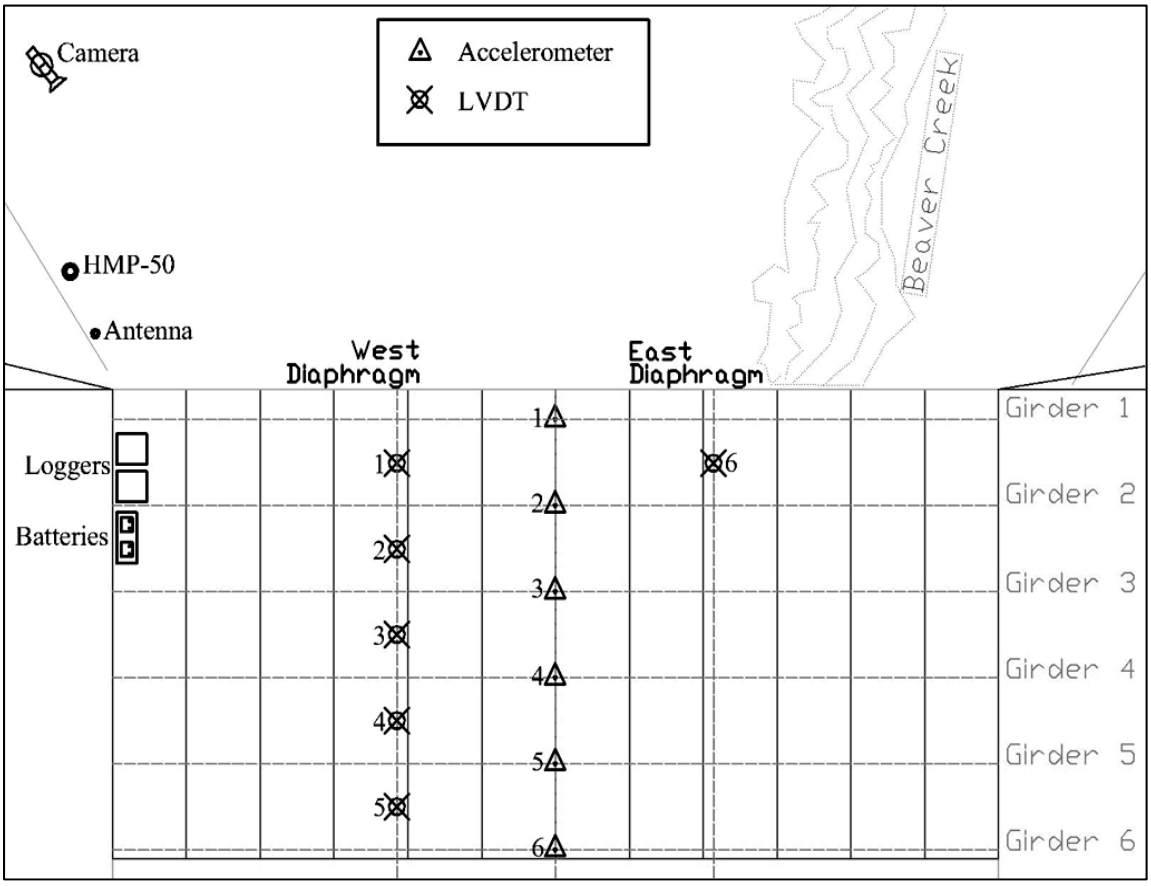

Figure 21. Instrument locations on the bridge as a whole

Figure 22. Location of camera with respect to bridge

2.4 Data Acquisition and Remote Data Transfers

Data acquisition for this project took many forms. For the most part, data were recorded using one of three data loggers; however, occasionally, data had to be taken manually. This section will provide a brief overview of the equipment used during this project and the different setups for data acquisition and transfer.

This project employed the use of three data loggers, two CR3000 Microloggers® and one CR1000 Measurement and Control Datalogger. The two CR3000 Microloggers were designated “A” and “B”. This project also used three RF401 900-MHz Spread-Spectrum Radios for transmitting real-time data from the loggers to the laptop during the panel lifting and moving procedures. It also used an AVW200 Vibrating-Wire Interface for exciting and measuring the VWSGs, and three AM16/32a 16-channel or 32-channel Relay Multiplexers (MUX) which increased the capacity of sensors simultaneously

connected. The specifications of above-mentioned equipment can be found on the Campbell Scientific™ website.

During this project, the three data loggers have had four different arraignments. The first setup was for the initial lifting of the panels removing them from their form work one at a time. Here both CR3000s were use to collect strain gauge data from the foil gauges at a sampling rate of 10 hertz. Each CR3000 is capable of measuring 14 foil gauges. The data were recorded to the memory on the logger but also broadcast in real time to an onsite laptop via a network of RF401radios, as seen in Figure 23.

During the second setup, each of the two instrumented panels were moved simultaneously to the bridge site. Each panel was issued one CR3000, one AM16/32a multiplexer, and one RF401. Thirteen of the 28 foil gauges on each panel were hooked directly to the CR3000; the rest were connected to the CR3000 using the multiplexer. Due to a mistake in the wiring scheme, the data from the multiplexers were lost, and only the data from the 13 sensors connected directly to the logger were recorded. The data from both panels were recorded to the memory of the loggers. Panel P2-05 was monitored in real-time during its transportation. Monitoring took place from a van which followed the flat-bed trailer at a safe distance, and communicated with the logger via a network of RF401radios, as seen in Figure 24.

To record the strains induced by posttensioning, all VWSGs were connected to the CR1000 via the AVW 200 and two multiplexers. The loggers were left running at the site the night before posttensioning began, and retrieved two days later. Additionally, as a backup, before and after posttensioning, data were taken manually from the VWSGs using a Geokon GK-401 Vibrating Wire Readout Box. The GK-401 excites the sensor

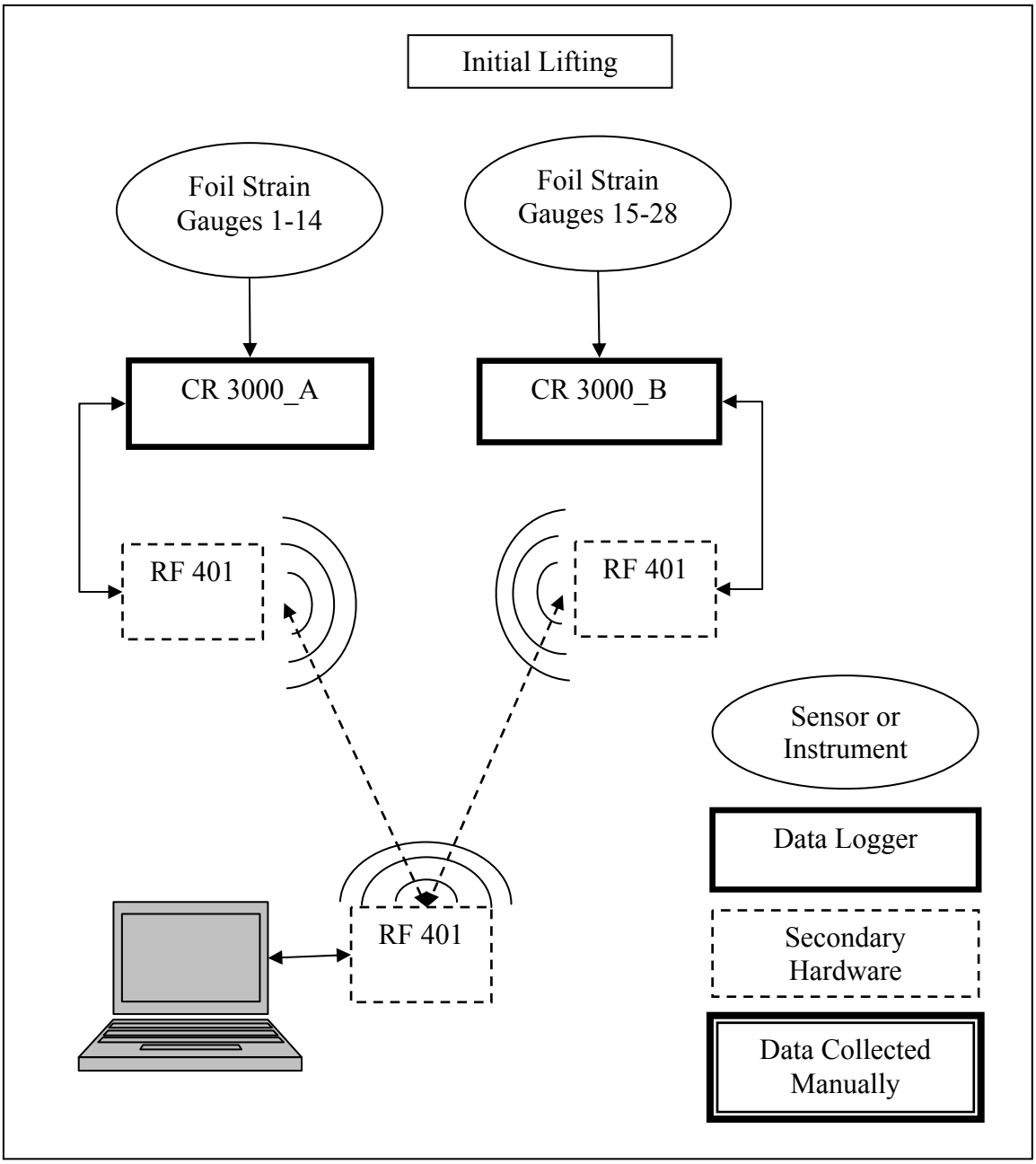

Figure 23. Equipment setup for initial lifting

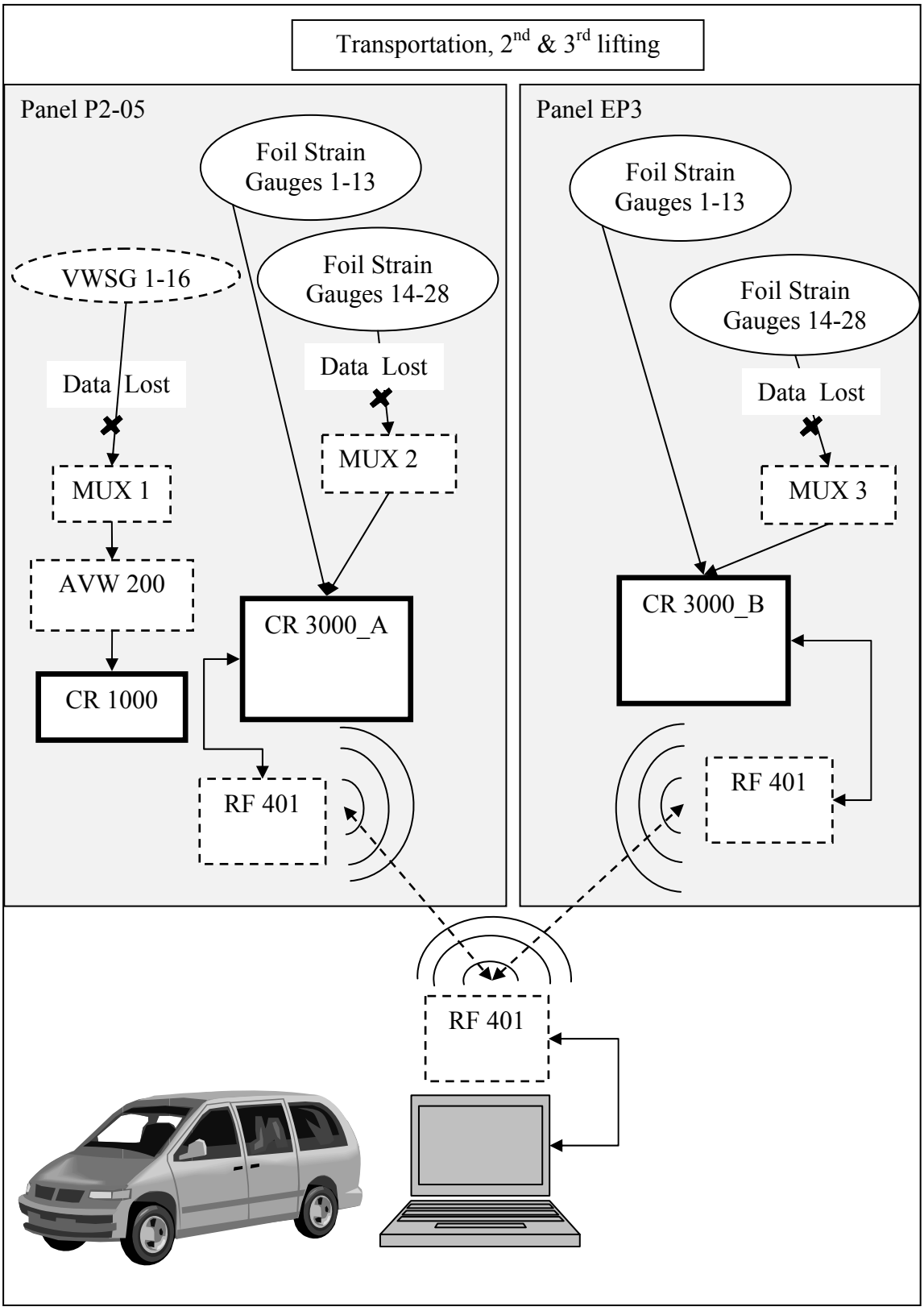

Figure 24. Equipment setup for transportation, 2nd and 3rd lifting

and measures its strain. An ohm meter was used to measure the resistance in each of the thermistors which corresponds to a temperature. Once data analysis began, it became evident that the data recorded on the logger were erratic, and the manually taken data from the GK-401were used instead.

Data acquisition during the truck load test and long-term monitoring used very similar setups but used different sampling schemes. During the truck load test, the VWSGs data were collected manually for each of the static truck load tests. Baseline data for the VWSGs were also taken. The six LVDTs were connected to CR3000A with a sampling rate of 1 Hertz. The CR3000 can only support 4 accelerometers each; as a result, the sensors had to be split up with four of the accelerometers attached to CR3000A, and the remaining two on CR3000B. The CR1000 recorded the atmospheric data taken hourly by the HMP-50. The accelerometers recorded all activity during the dynamic truck load tests at a rate of 50 hertz. Finally, during each static truck load test, the deflections of the girders were recorded using surveying equipment. Baseline data were also taken. The truck load test and long-term setups are visualized in Figure 25.

The long-term data acquisition set up was the same as the truck load test setup with the following exceptions. The data loggers are powered by two twelve volt car batteries; the batteries are charged using two solar panels and a voltage regulator. The VWSGs were connected to the AVW200 via two AM16/32a multiplexers, the AVW200 was connected to the CR1000 along with the HMP-50, and these data were sampled every 2 minutes, and then averaged and recorded every 3 hours. The sampling rate of the LVDTs remained at 1 Hertz and was averaged and recorded in 3-hour periods. The camera is connected to the CR3000B, the same one as accelerometers five and six.

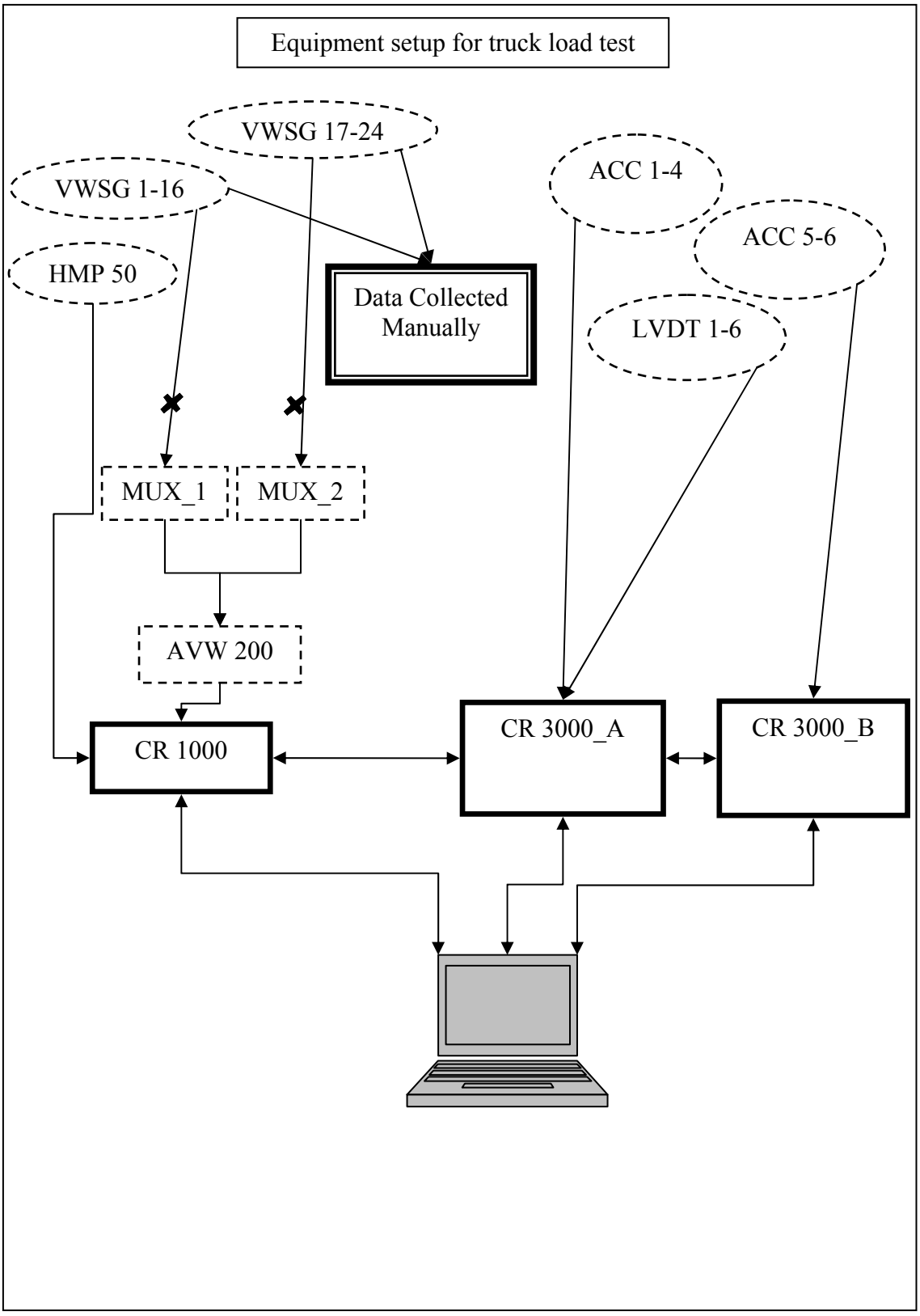

Figure 25. Equipment setup for truck load test

The camera is triggered whenever the acceleration of accelerometer five goes above 25 milli gs. Long-term accelerometer data are acquired in two ways: first, the data loggers record the largest acceleration each day and the time of day when it occurred. Second, whenever accelerometer four or five read above the 25 milli g threshold, a series of data is recorded in which 50 samples before the event and 250 samples following the event are recorded. Together with the camera, this setup provides a picture as well as an acceleration signature every time accelerometer five exceeds the 25 milli g threshold.

The three data loggers are connected to each other through their COM ports, allowing them to communicate with each other. The modem and subsequent antenna are connected to CR3000B which allows the laptop to access any of the data loggers from anywhere an internet connection is available, as seen in Figure 26. Remote access via the laptop allows the user to receive and send programs changing the sampling rate or sampling scheme; it also allows the user to collect data stored on the loggers, manually trigger the camera, and monitor any of the sensors or battery voltage in real time.
Many different Campbell Scientific software have been used during this project. RT-DAQ was used for monitoring the lifting strains in real time due to its high refresh rate. Loggernet was used for accessing the loggers remotely, which provided access to download data tables, uploaded new programs for the loggers to run, monitored the bridge from offsite, and manually triggered the camera. The program Ace Manager was used for configuring the camera. Two programs were used for the compilation of data logger programs, Short Cuts and the CR Basic Editor. Lastly, a program called the Device Configurations utility was used to configure the loggers for use with all secondary hardware.

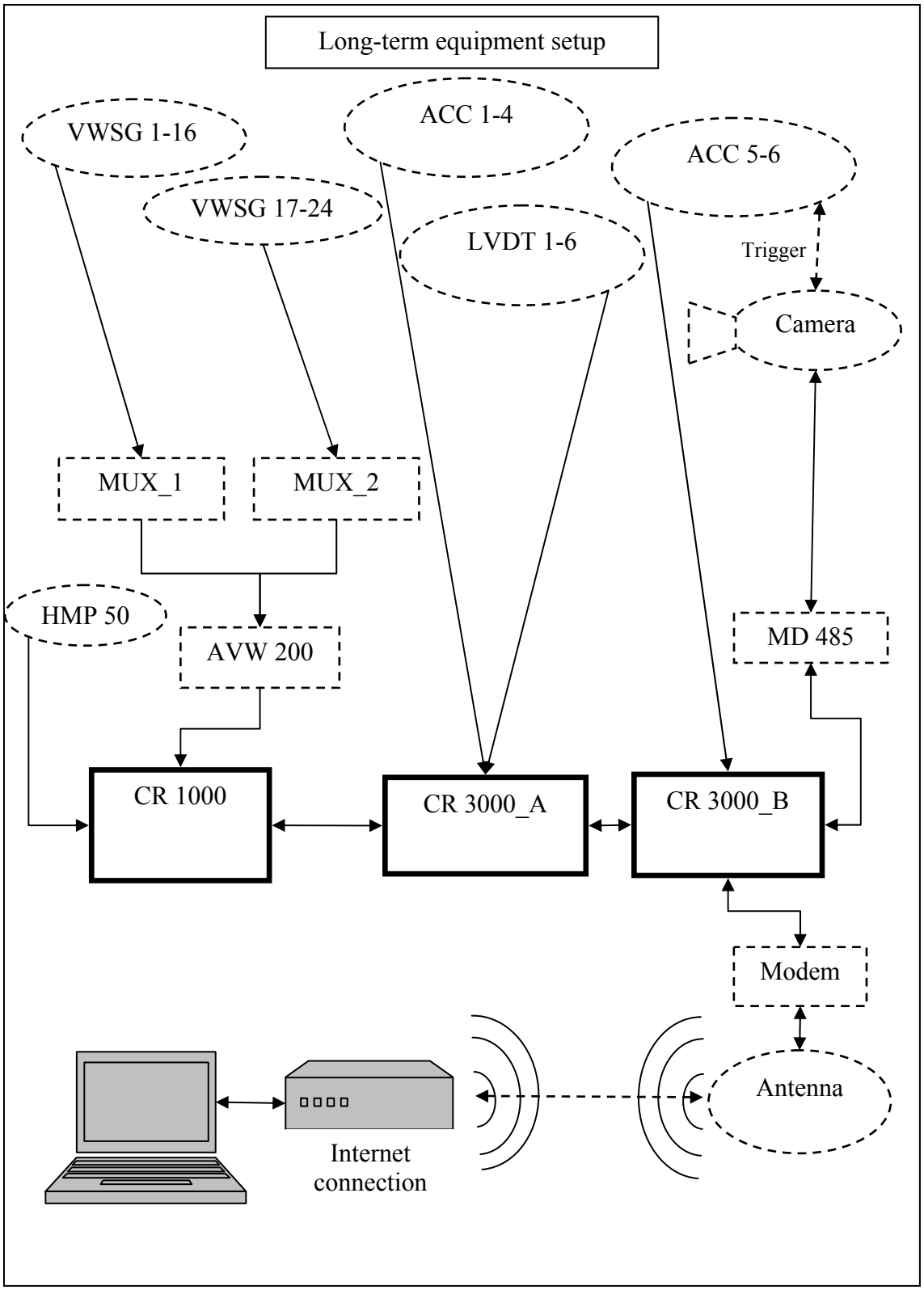

Figure 26. Equipment setup for long-term monitoring.

CHAPTER 3

EXPERIMENTIAL OBSERVATIONS

3.1 Experimental Observations for Lifting and Transport

3.1.1 First Lift

Panels P2-05 and EP3 underwent their first lifts on July 27th and August 6th 2009, respectively. The lifts occurred before the parapets had been cast. The panels were lifted from their formwork at four points. The maximum strain profile for half of the panel P2-05 is shown in Figure 27. From the graph, we can see that the maximum strain in the bottom matt is 125 μstrain while the maximum strain in the top matt is 50 μstrain. The maximum strain of 125 μstrain corresponds to 0.8% of the ultimate GFRP strain. The lifting points are located at 46 in. and 202 in. from the parapet, and are represented by arrows.

3.1.2 Second Lift

The panels were transported from the precaster to the bridge site on September 3rd, 2009. The transportation process involved two lifts (referred to as lifts two and three), and a 64-mile journey on the back of a long flatbed trailer. At this point, the parapets on both panels had been cast. Due to scheduling complications and a wiring mistake, the data from this day are limited to the first thirteen stain gauges on each panel. The

maximum strain profile during the second lift for half of panel P2-05 is shown in Figure 28. From the graph, we can see that the maximum strain in the bottom matt is -45 μstrain while the maximum strain in the top matt is approximately 30 μstrain. The maximum strain of -45 μstrain corresponds to 0.3% of the ultimate GFRP strain. The lifting points are located at 46 in. and 202 in. from the parapet, and are represented by arrows. Overall the strains observed during the second lift were insignificant.

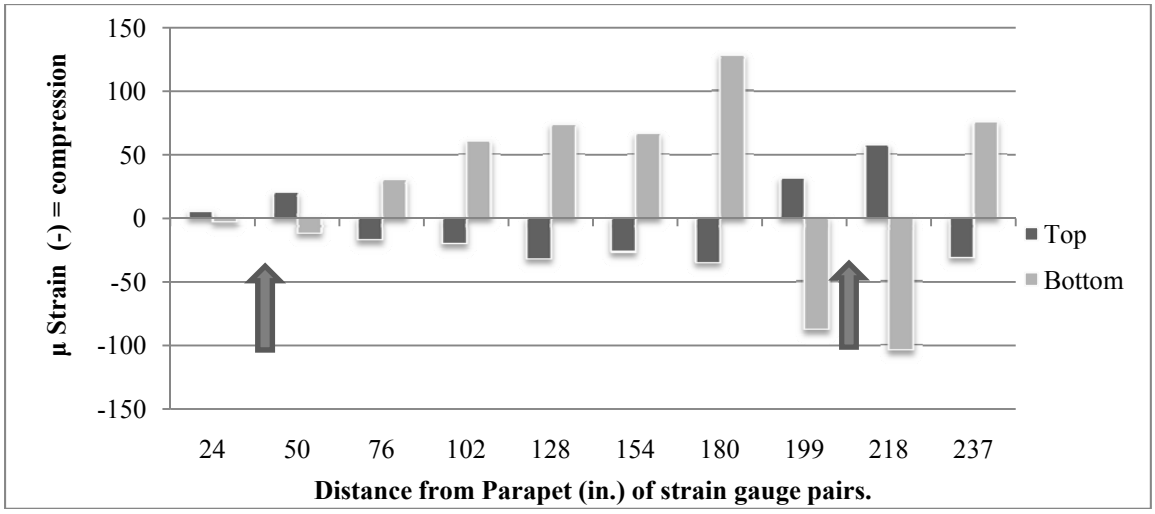

Figure 27. Strain profile for P2-05 during its first lift removing it from the formwork

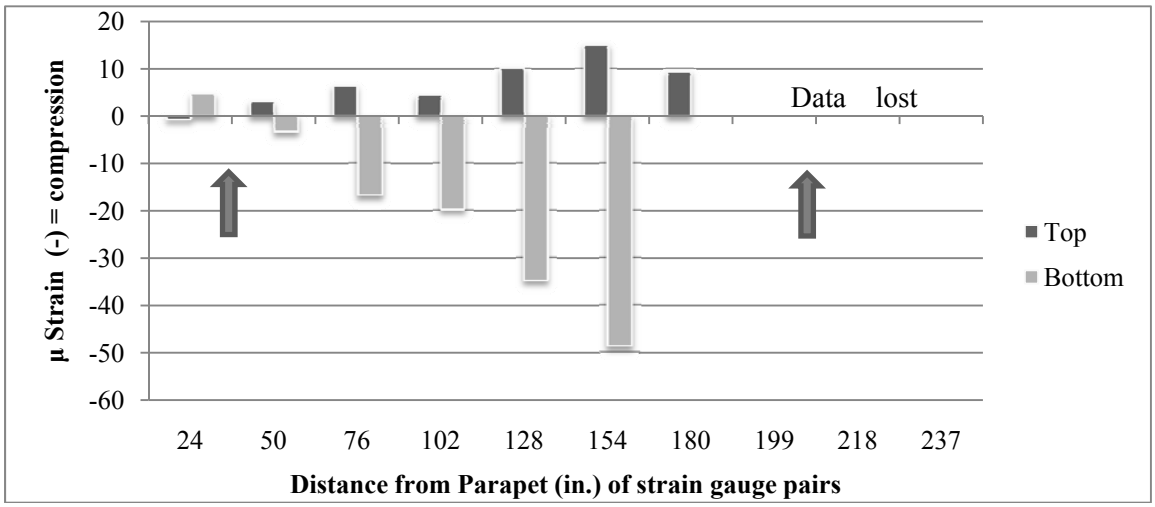

Figure 28. Strain profile for panel EP3 during its second lift

3.1.3 Transport

After the panels were placed upon the trucks, the trucks began a 64-mile journey to the bridge site. The maximum, minimum, and average of all the strain gauges during the journey is shown in Figure 29. During transport of panel EP3, careful observations were made and correlated to the strains on the graph. Long-term observations, on the order of hours, have resulted in trends that represent a floating nature of the foil strain gauges. After the panels third lift placing it upon the bridge girders, one would expect the strains in the panel to decrease back to their initial values; however, this was not observed. The causes of these long-term changes are most likely due to temperature effects. Nevertheless, from the graph, it can be seen that the maximum strain for the entire day did not surpass 60 μstrain in ether tension or compression. The maximum strain of -52 μstrain corresponds to 0.3% of the ultimate GFRP strain.

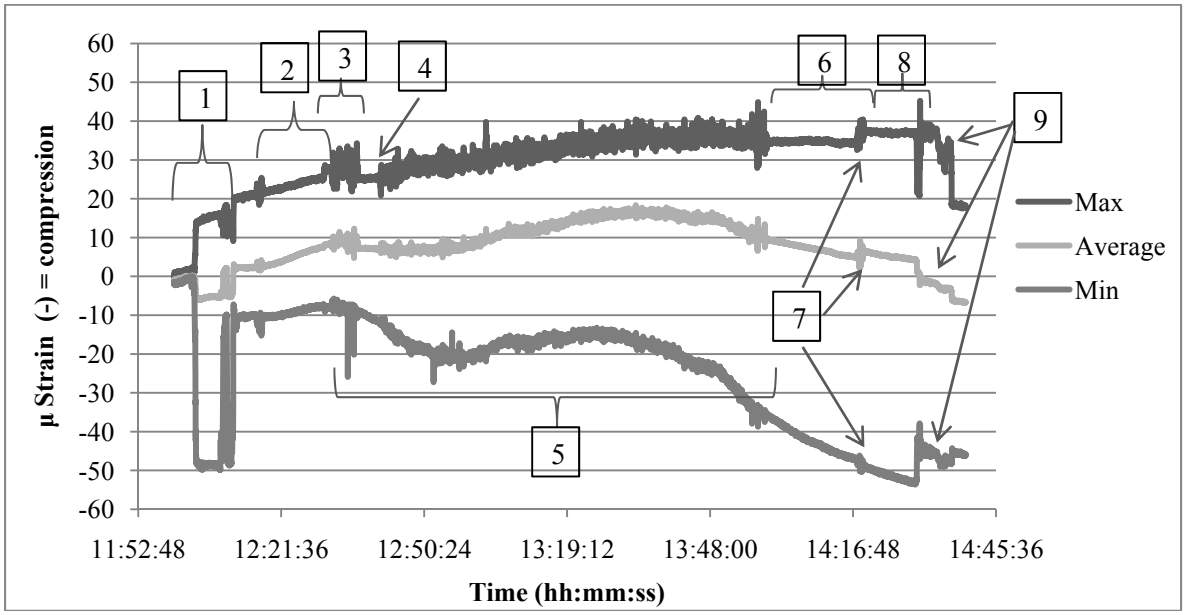

Figure 29. Max, min, and average in all gauges during lifting and transport of panel EP3

The following observations were made during the day panel EP3 was moved to the bridge site:

1. The second lift, placing the panel on the truck.
2. Truck is stationary while panel is strapped down and straps are tightened, resulting in slight increase in strain.
3. Truck begins to move through the precast yard and out of Pleasant Grove.
4. Truck is stationary while waiting to get on the Freeway
5. Truck travels the 64 miles to the bridge site.
6. Truck arrives at the bridge site and remains stationary until it is unloaded.
7. Truck maneuvers the construction site and moves into position.
8. Straps are removed.
9. Panel is lifted into place.

3.1.4 Third Lift

The maximum strain profile during the third lift is shown in Figure 30. The third lift occurred directly after the transportation of the panel, resulting in added difficulty in acquiring base line data. From the graph, we can see that the maximum strain in the bottom matt is -45 μstrain while the maximum strain in the top matt is -35 μstrain. The maximum strain of -45 μstrain corresponds to 0.3% of the ultimate GFRP strain. The strains for all three lifts were in the same range, and never exceeded 125 μstrain, or 0.8 % of the ultimate GFRP bar strain.

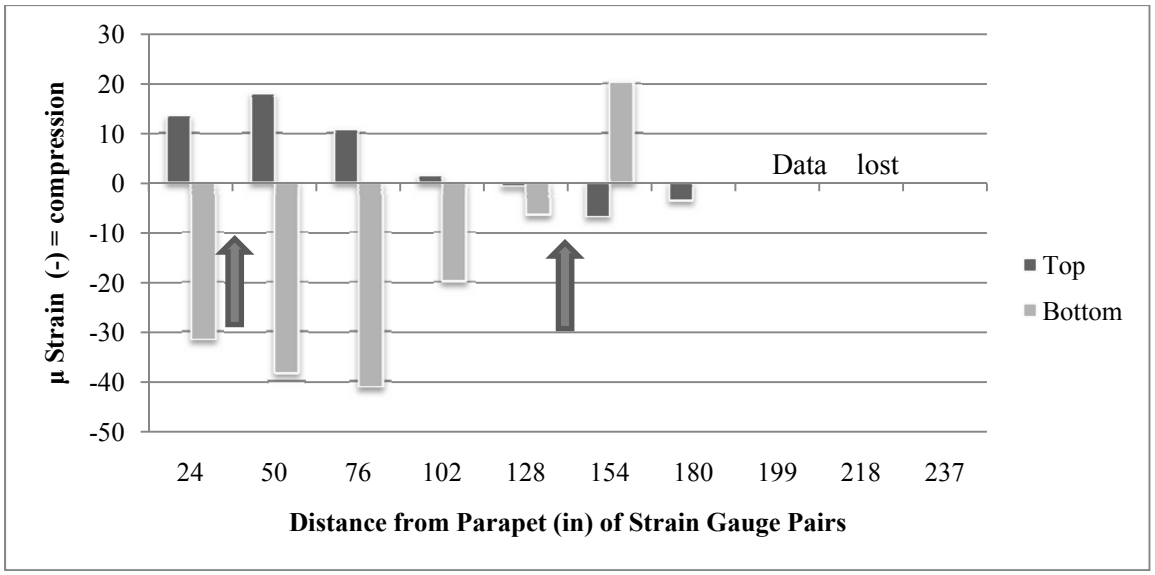

Figure 30. Strain profile for EP3 during its third lift

3.2 Posttensioning Observation

The Beaver Creek Bridge is the first bridge deck in the state of Utah to be posttensioned. Posttensioning of the bridge deck was conducted on September 17th, 2009. Posttensioning consisted of eleven pockets. Each pocket was made up of three 0.6 in. (15mm) Grade 270 (1862MPa) low relaxation steel strands. Once posttensioning had concluded, the strands and pockets were grouted. Originally, the posttensioning data were supposed to be recorded using the data loggers, allowing for the observation of the posttensioning process as well as the observation of following days when the majority of creep, shrinkage, and relaxation effects occur. However, due to a miscommunication in the wiring diagram, the data from the loggers was erratic, and the before and after data from the GK-401were used. As a result, the data on posttensioning presented in this paper include the effects of creep, shrinkage, and strand relaxation combined.

Before and after posttensioning, data were taken with the VWSGs in the longitudinal direction. The change in strain with temperature adjustment is displayed in Figure 31. The odd numbered gauges are located in the same horizontal plane as the top mat of GFRP reinforcing while the even numbered gauges are located in a similar fashion with the bottom mat. Gauges 1-4 are located on panel EP3 and gauges 5-8 are located on panel P2-05, as seen in Figure 32.

The average concrete strain from all 8 gauges is approximately 130 μstrains in compression. However, the average concrete strain for panel EP3 is 112 μstrains, almost 30 μstrains lower than those found in panel P2-05 where the average strain was 141 μstrains. Approximately the same difference in strain was found when comparing the averages of the top gauges to those of the bottom gauges. This difference is most likely due to the camber of the bridge.

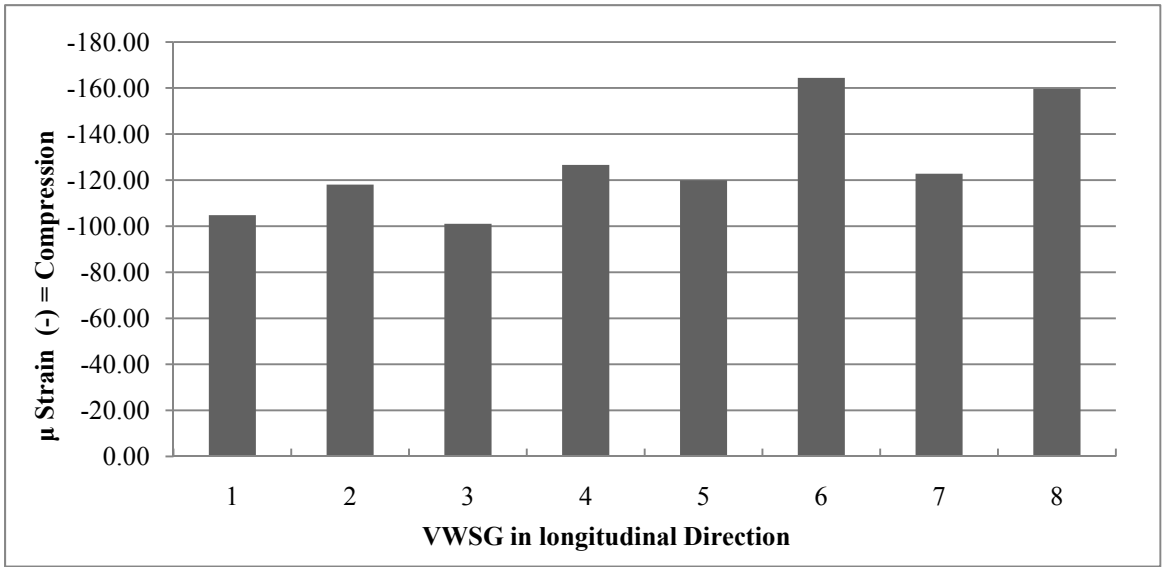

Figure 31. Posttensioning strains in bridge deck

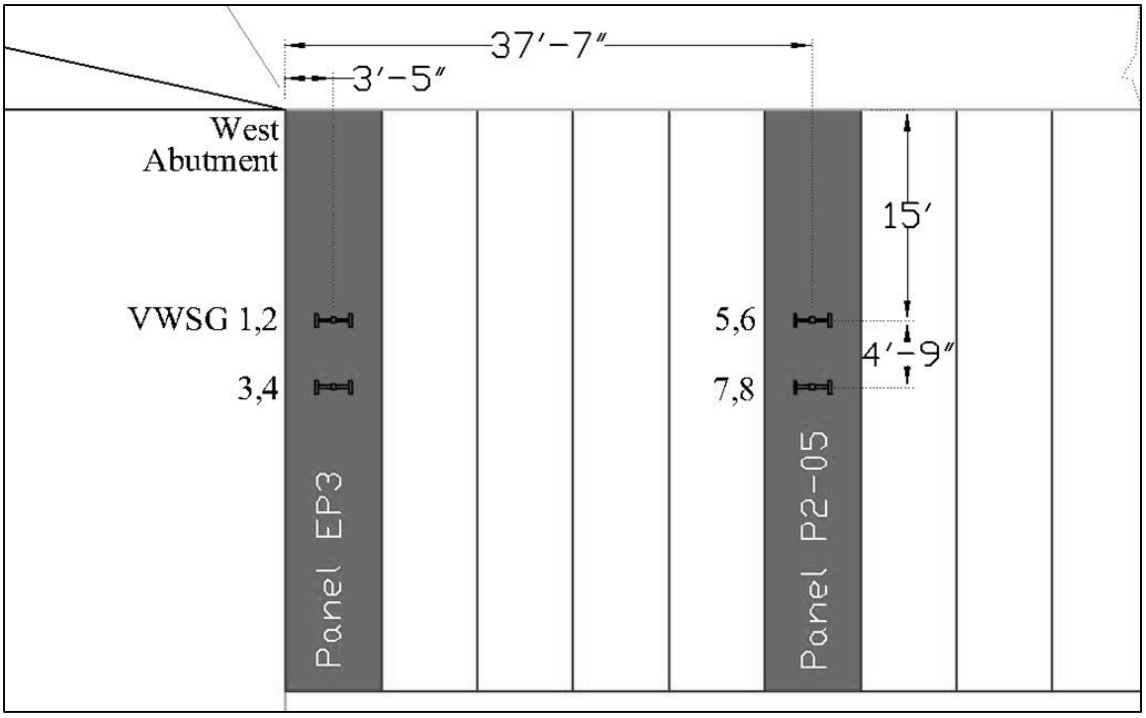

Figure 32. Locations of posttensioning VWSGs

3.3 Truck Load Test Observations

The truck load test was performed on September 29th 2009. During the static tests, three types of data were collected. Internal concrete strains were collected from the vibrating wire strain gauges, deflection data of the deck panels relative to the girders were collected using LVDTs, and girder deflection data were collected using surveying equipment.

3.3.1 VWSG

The maximum compressive and tensile strains in the concrete occurred during Test 2 when truck "A" was directly over the right lane. The maximum compressive and tensile strains were -176 μstrains and 18 μstrains, respectively, as seen in Figure 33. The tensile strains observed throughout the static truck load tests were small and only

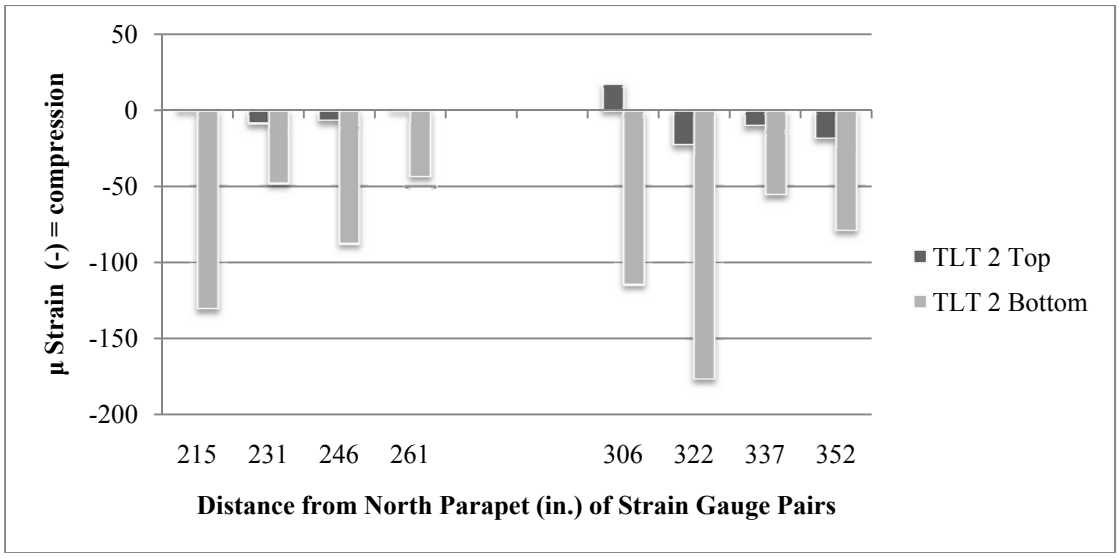

Figure 33. Strains from the VWSG for truck load test 2

observed in the top of the panel. The majority of the sensors were in compression throughout the truck load tests. The only gauge to exceed 150 μstrain was VWSG #20. On the whole, the strains observed in the concrete during the truck load test were not significant. It is believed that the loads were insignificant when compared to the capacity of the deck. The strains observed in the concrete during the truck load test were larger than those observed in the GFRP bars during the lifting and moving procedures. However, the truck load test strains were still small with respect to the capacity of the deck.

3.3.2 LVDT

As expected, the maximum panel deflections occurred during truck load test #9 when both trucks were parked above the west diaphragm. The maximum deflection was 0.007 in. relative to the girders, as seen in Figure 34. This was well below the AASHTO limit of L/800, or in this case 83”/800=0.104”.

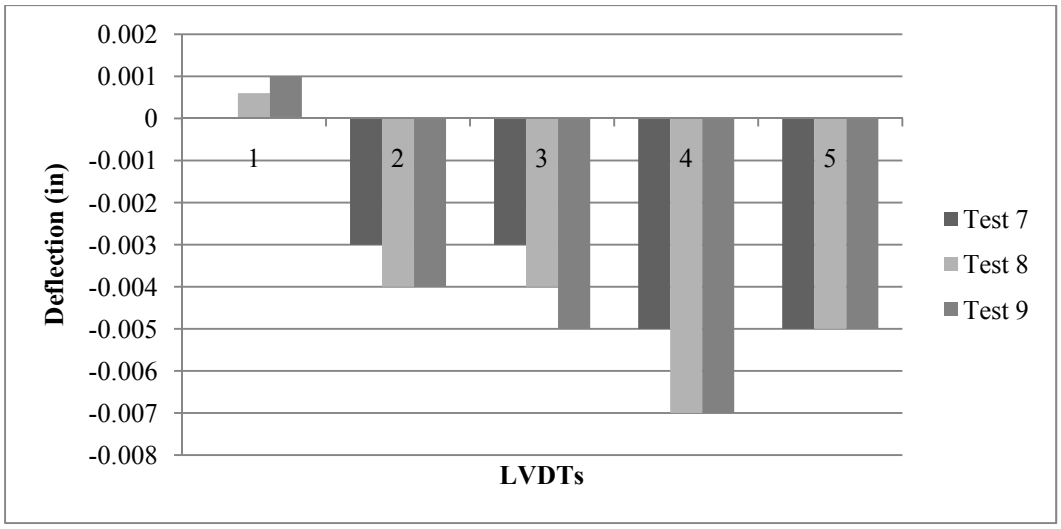

Figure 34. Panel deflections relative to the girders above the west diaphragm

3.3.3 Girder Deflections

As expected, the maximum deflection of the girders occurred during truck load test #8 when both trucks were parked at the bridge midspan. The maximum deflection was 0.13 in. as seen in Figure 35, recorded in girder 4 located between the two trucks. The peak deflection of 0.13 in. was well below the AASHTO limit of L/800, or in this case, 1058 in./800=1.32 in.

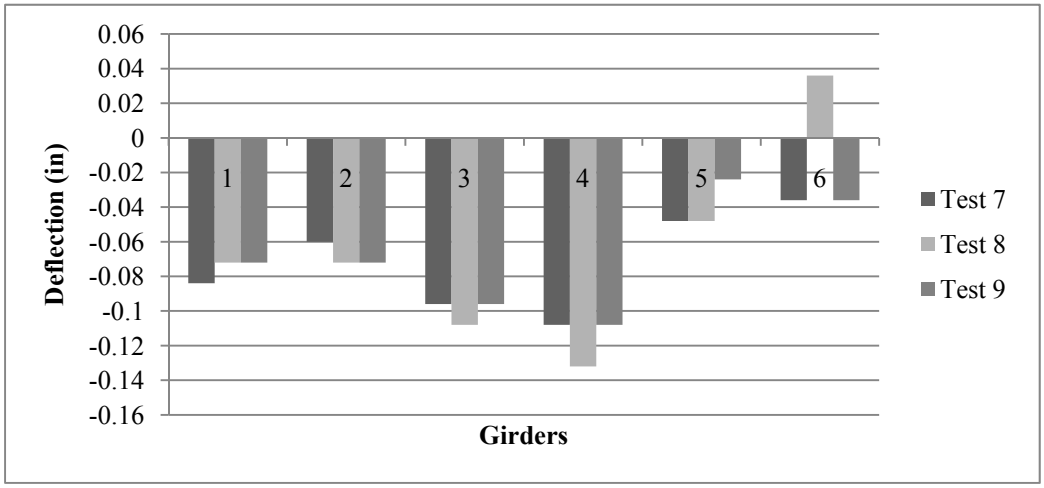

Figure 35. Midspan girder deflections for tests 7 through 9

During truck load test 9, additional girder displacements were measured above the west diaphragm. This was done to correlate girder deflections and panel deflections at the same point. Additional deflections data were taken for girders two and three, as seen in Figure 36. The deflection of the diaphragm is assumed to be linear between the girders. The displacement of the diaphragm at midspan between girders two and three was calculated to be 0.06 in. Combining this with the panel deflection from LVDT #2 for the same test, the total deflection of the panel located above LVDT #2 has been calculated to be 0.064 in. The relative deflection of the panel with respect to the least deflected girder can be determined using half the difference between the two girders and deflections data from LVDT #2. Doing so results in a deflection of 0.016 in. relative to girder 3. Both these values are below the AASHTO limit of 0.101in.

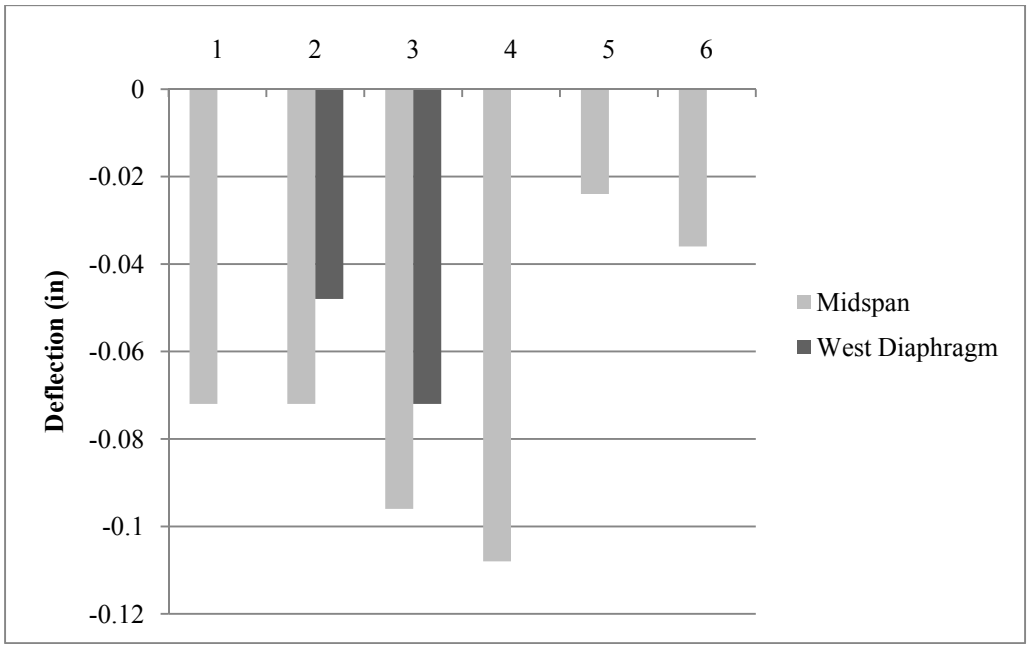

Figure 36 Girder deflections for truck load test 9

3.3.4 Accelerometers

Dynamic tests result in an acceleration profile similar to the one shown in Figure 37. Peak accelerations are caused as the truck travels across the bridge. It takes the truck approximately one second to cross the bridge. The settling time for residual vibrations is approximately five seconds.

During the 40 mph and 35 mph dynamic tests, the maximum acceleration was found toward the sides of the bridge in girders 1, 5, and 6, as shown in Figure 38. It is theorized that during these tests, the trucks were going slow enough to act as a damper, and reduce the peak accelerations on girders 2 through 4.

During the faster tests, preformed at 65 mph, the maximum acceleration was found directly below each truck in its respective lane, as shown in Figure 39. The maximum acceleration for the entire dynamic test occurred during test 11, when truck B passed over the left lane of the bridge traveling at 40 mph.

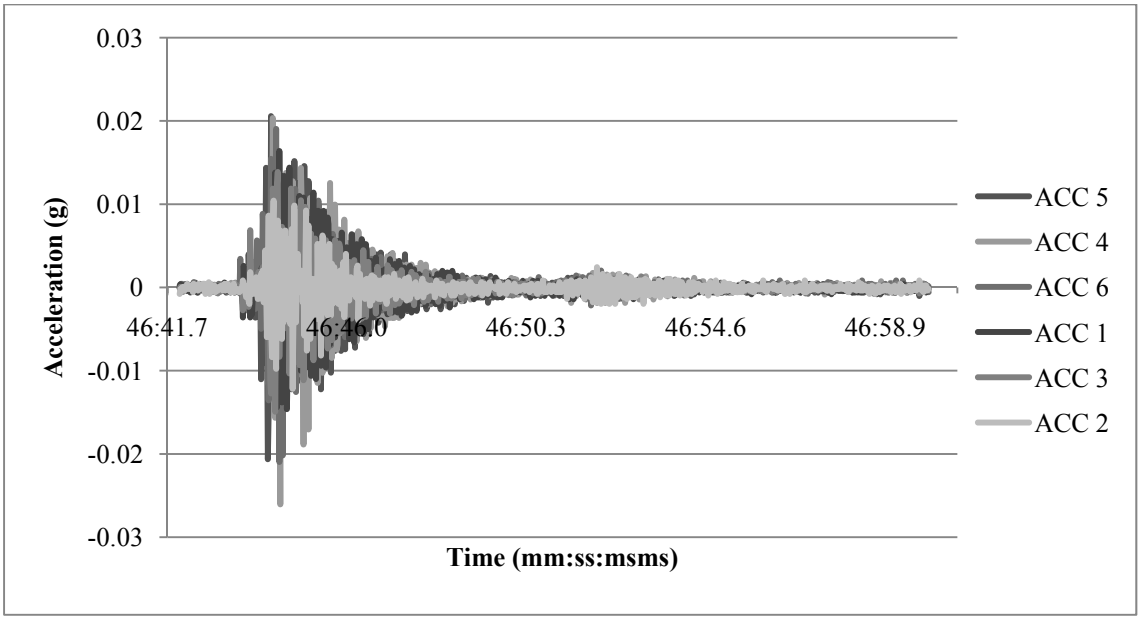

Figure 37. Typical acceleration profile for dynamic tests; this profile is from test 14

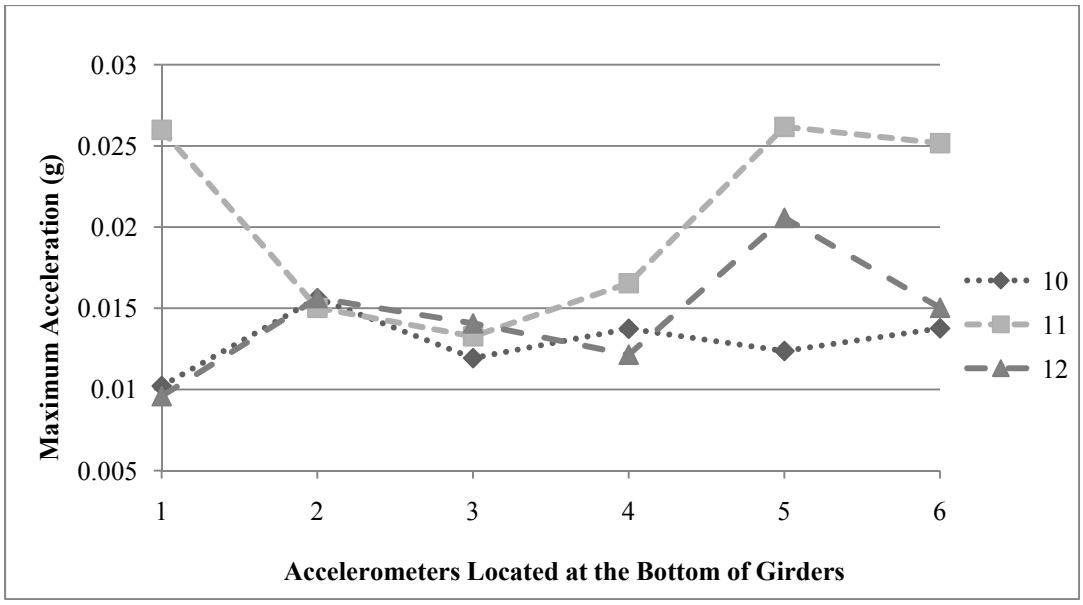

Figure 38. Peak accelerations for dynamic tests performed at 35 and 40 mph

Figure 39. Peak accelerations for dynamic tests performed at 65 mph

CHAPTER 4

ANALYTICAL RESULTS

4.1 Comparison of Lifting Curvature Diagrams with PCI

The lifting of each panel took place in accordance with the PCI design handbook fifth edition. PCI predicts the moment felt by the panel should be equal to 43.9 kip-in from Eq. (1), where "w" is the weight of the panel per square foot, and "a" and "b" are the dimensions of the panel. Figure 40 defines "a" and "b" and shows the theoretical bending moment diagram. The panels were lifted at different points, and it should be expected that the moment diagram is different with similarities in shape. From the moment diagram predicted by PCI, the theoretical curvature can be calculated using Eq. (2), where "M_t" is the moment calculated from Eq. (1), "E" is the modulus of elasticity and "Ie" is the effective moment of inertia. Typically, in this equation, the gross moment of inertia "Ig" is used; however, this assumes the cross section of the panel is still completely intact without any cracks; this is not the case.

Recent work done by Ruifin Liu at the University of Utah (Ruifin Liu, personal communication, February, 2011) has concluded that panels which have yet to see any loading already have a reduction in their gross moment of inertia, due to shrinkage, handling, and self weight stresses. The reduced moment of inertia ranges from 20% to 40% of the gross moment of inertia.

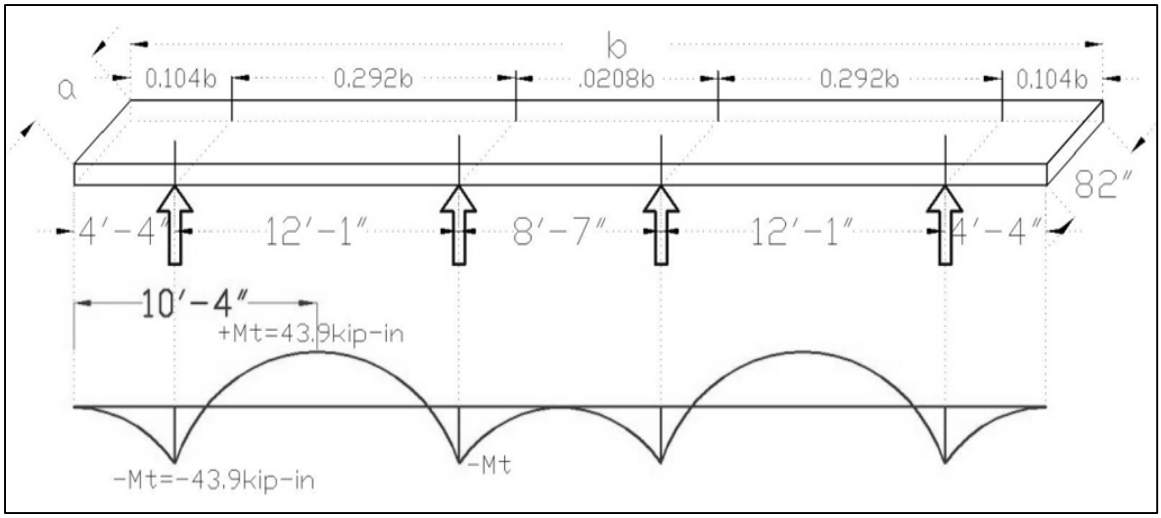

Figure 40. Lifting points and moment diagram from PCI design hand book 5th edition

Using a moment of inertia equal to 0.2 Ig and Eq. (2), the theoretical curvature "φ" has been calculated to be 9.05×10^{-6} /in. Moreover, using a moment of inertia equal to 0.4 Ig, the theoretical curvature has been calculated to be 4.51×10^{-6} /in.

$$-M_t = +M_t = 0.0027 * w * a * b^2 \quad (1)$$

$$\varphi_{calc} = \frac{M}{EI_e} \quad (2)$$

From the recorded strains during lifting, the curvature of the panel was determined using Eq. (3), where "ε" is the strain recorded and "d" is the distance between the top and bottom reinforcing mats. The measured curvature diagram from the first lift of P2-05 is shown in Figure 41, along with two arrows representing the closest lifting points. The theoretical curvature will be compared to the measured curvature at three points, under each lifting point, and at midspan between the two lifting points.

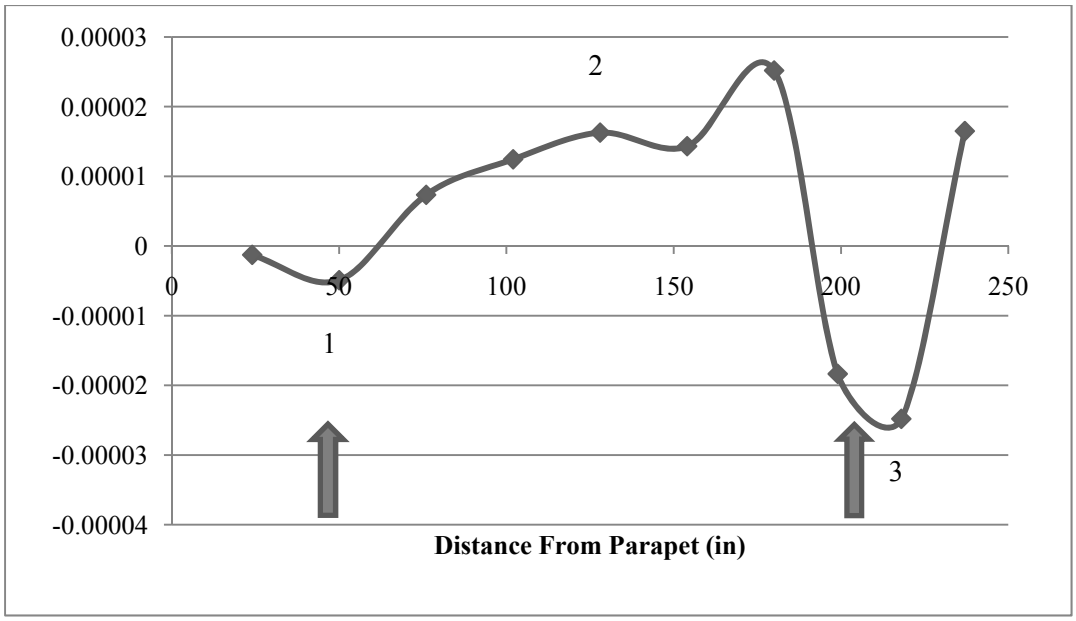

Figure 41. Curvature diagram from experimental results; arrows represent lifting points

The curvature under the first lifting points is 4.9×10^{-6} /in. and is within the range of theoretical curvatures. At the midpoint between two lifting points, the curvature is 1.63×10^{-5} /in. which is 1.6 times the upper limit of the theoretical range. The curvature under the second lifting point is 2.5×10^{-5} /in. and is 2.7 times the upper bound of the theoretical curvature. The difference between the theoretical and measured curvature is thought to come from fixed end moments induced by uneven lifting. The panel was lifted at four points and underwent uneven deformation due to different vertical forces in the cables. The different vertical forces strained the lifting cables differently, creating a scenario similar to that found when a multispan beam undergoes uneven settlement at its supports, thus creating fixed end moments at each support.

$$\varphi_{measured} = \frac{\varepsilon_{top} - \varepsilon_{bottom}}{d} \quad (3)$$

4.2 Posttensioning

The posttensioning cables were each tensioned with a force of 40.8 kips. The total jacking force from all the strands on the Phase 2 side of the bridge was found to be 1346 kips. From the initial jacking force of the posttensioning strands, the stress in the slab was calculated simply dividing by the cross section of the panel, and determined to be 295 psi. Using the modulus of elasticity of the concrete, the theoretical change in strain of the concrete was found to be 62 μstrains, as seen in Eq. (4). This is approximately half the average of 130 μstrain recorded by the VWSGs. However, the recorded values also take into account other strains such as creep and shrinkage.

$$\frac{\text{Total Jacking Force}}{(\text{Cross Section Area})*(\text{E}_\text{c})} = \frac{\frac{40.8 kips}{strand}*\frac{3\ strands}{pocket}*11\ pockets}{(4572\ in^2)*(4.675*10^6 \text{psi})} = 62\ \mu\ strain \quad (4)$$

4.3 Panel Deflections

During the design of the bridge, the deflection of the panel relative to the girders was calculated using the HL-93 design loading and the deflection equation from the ACI 440.1R-06 example (Eq. 5). The deflection of the deck relative to the girders due to positive live load moment was calculated to be 0.101 in. (Rebecca Nix, personal communication, July, 2009). The maximum deflection of the panels relative to the girders recorded during the truck load test was 0.007 in, 93% less than the design deflection. Furthermore, the peak deflection of 0.007 in. was well below the AASHTO limit of L/800, or in this case 0.101 in. Taking into consideration that the truck load test involved lighter trucks, the deflections are small enough to suggest that the changes made to the design of the bridge were successful in maintaining small service deflections.

$$(\Delta_i)_{LL} = \frac{5*M_{LL}*{l_{eff}}^2}{48*E_c*(I_e)_{LL}} = \frac{5*(5.56\ kip\ ft)*(83\ in)^2}{48*(3.834*10^3\ Ksi)*123.223\ in^4} = 0.101in \quad (5)$$

4.4 Girder Deflections

The maximum deflection of the girders was 0.13 in., and it occurred during truck load test 8. This was well below the AASHTO limit of 1.325 inches. During truck load test 8, the trucks were positioned primarily over girders 3, 4, and 5; however, girders 1 and 2 were each deflected 0.07in., and girder 6 deflected upward 0.03 in. The small deflections observed across girders 1 through 5, and the positive deflection observed in girder 6, provides additional evidence that panel-girder continuity was achieved via the blockouts. Moreover, the panels were successful in transferring live loads evenly among the girders.

4.5 Accelerometers

It was expected that the tests involving faster moving trucks would also correlate to higher accelerations; this turned out not to be the case. As seen in Figure 42, the maximum accelerations of faster moving trucks were no higher than those at lower speeds. The trend line drawn in the graph does represents a positive correlation. However, the R-squared value is only 0.283, meaning that there is little correlation between velocity and maximum accelerations at midspan. Given the nature of the accelerometer data, it is difficult to hypothesize on potential trends, and more data are needed before a firm conclusion can be drawn.

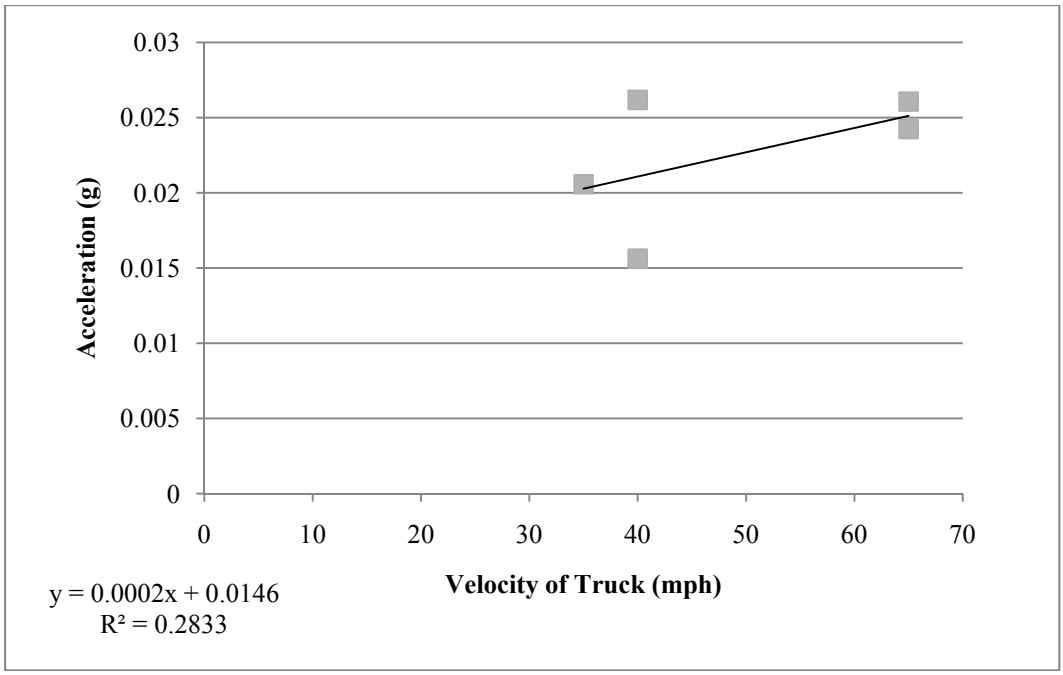

Figure 42. Correlation between maximum acceleration observed during dynamic test and velocity at which test was performed

4.6 Cost Analysis

The cost differential of new materials is of the utmost importance. Cost data from the Beaver Creek Bridge and a similar size RC steel bridge were provided by (Rebecca Nix, personal communication, October, 2010), bridge engineer at UDOT. The two bridges were constructed in close temporal proximity to each other. The use of GFRP reinforcing bars increased the overall capital cost of this bridge by 8%. However, further investigation into the per-year cost of the bridge deck is required due to the noncorrosive nature of the material, and the extended design life the material provides.

The cost of the GRFP and steel deck was $59.25 /sq. ft. and $49.06/sq. ft., respectively, a 21% increase. The Beaver Creek Bridge also had two additional girders to accommodate the GFRP deck, resulting in an additional cost of $48,000. When applied to the cost of the deck, the additional girders resulted in an additional $6.82/sq. ft., bringing

the total cost of the GFRP deck up to $66.07/sq. ft. Altogether, the GFRP deck cost 35% more than the traditional RC steel deck. However, there is more to a bridge than just its initial cost. The design life of the Beaver Creek Bridge was 60 years compared to the 45 years of the RC steel bridge. The 60 year design life is a conservative estimate since there is little historical data. The cost comparison on a per year basis is less dramatic, resulting in $1.10/sq. ft./yr for the GFRP deck and $1.09/sq. ft./yr of the steel deck, as seen in Table 6. The use of GFRP will also result in less scheduled maintenance and fewer resultant user delays.

Recent work investigating the durability of GFRP bars (Weber and Baquero 2010) recommends increasing the design life of GFRP decks to 100 years. Changing the design life to 100 years provides a per-years cost of $0.66 /sq. ft/yr, as seen in Table 6. The extended design life of the GFRP deck provided a monetary advantage over traditional steel RC decks, despite its higher initial capital cost.

Table 6. Cost analysis

	Beaver Creek GFRP bridge		R/C Steel bridge	
	As built	Extended design life	As built	Extended design life
Deck cost (/sq. ft.)	$59.25	$59.25	$49.06	$156
Additional girders	$48,000	$48,000	$0	$0
Girder cost (/sq. ft.)	$6.82	$6.82	$0	$0
Design life (years)	60	100	45	100
Cost per year (/sq. ft./yr)	$1.10	$0.66	$1.09	$1.56

CHAPTER 5

CONCLUSIONS

This project monitored two Glass Fiber Reinforced Polymer deck panels for the Beaver Creek Bridge on US 6. The panels were monitored through every step of construction, from fabrication of the panels in the precast yard, through three lifts, and transportation. The completed bridge at Beaver Creek underwent a truck load test, and is now being monitored in service through a separate project. From the measurements and observations taken during this project, the following conclusions can be drawn:

1. The panels and bridge were successfully instrumented. During lifting and transport, the data loggers transmitted live data to an onsite laptop, where the strains in both the top and bottom GFRP mats were monitored in real-time. Additionally, the data loggers were successfully setup for automatic data acquisition for use during the truck load test and during long-term monitoring.
2. To minimize stresses, the panels were lifted at four points using straps, supporting the panels from below. The maximum tensile strain in the GFRP bars was 125 μstrain; this strain corresponds to 0.8% of the ultimate strain of 16,000 μstrain. The strains observed during this project were consistent with those reported by Benmokrane et al. (2006).

3. Analysis of the curvature diagrams for the panels during lifting was conducted. Using the reduced moment of inertia and Eq. (2), the peak theoretical curvature "φ" was calculated to be 9.05×10^{-6} /in. The maximum curvature for the lift is around 2.5×10^{-5} /in. By comparison, the maximum measured curvature of the panel is 2.7 times that of the theoretical curvature. The curvature at the other two points was more reasonable, with one point being within the theoretical curvature and another being 1.6 times the theoretical. Much of this difference is thought to be taken into account from differential deflections of the lifting points, resulting in additional fixed end moments.
4. The deck panels were posttensioned in the longitudinal direction of the bridge. The partial posttensioning in the longitudinal direction caused a maximum compressive strain of 164 μstrain, and an average strain of 130 μstrain. From the initial jacking force of the posttensioning strands, the theoretical change in strain of the concrete was calculated to be 62 μstrain. This is approximately half the average strain of 130 μstrain recorded by the VWSGs. However, the measured value includes other strain effects such as creep, shrinkage, and strand relaxation. It is believed that posttensioning added to the continuity of the bridge deck and increased the sheer transfer of the grouted keyways and allowing the panels to transfer much of the shear load to adjacent panels, thus reducing the deflections observed during the truck load test.
5. The bridge underwent static and dynamic truck load tests, in which the west bound lanes of the bridge were tested individually as well as simultaneously. During the static portion of the truck load test, the relative deflections between the

bridge deck and the west diaphragm were measured. The maximum magnitude of the relative deflections was found to be 0.007 in. which is small and shows that there was significant composite action between the deck panels, distributing the load from panel to panel. The design deflections, calculated using ACI 440, may have overestimated the deflections. The test deflection of 0.007 in. was 93% less than the design deflection of 0.101 in. However, the test loads were approximately 40% the design loads. Furthermore, the deflections were 7% of the AASHTO limit of 83/800= 0.104 in.

The live load deflections of the prestressed girders during the static truck load tests were found to be significantly smaller than the allowable deflection specified by the AASHTO Specifications (2009). The decreased girder spacing and resultant increase in the number of girders may accounts for this. For two trucks located at midspan weighing a total of 87.04 kips, the maximum deflection observed was 0.13 in. The small deflections observed across girders 1 through 5, and the positive deflection observed in girder 6, provides evidence that panel-girder continuity was achieved via the blockouts.

6. The changes made to the design of the bridge to accommodate GFRP bars were successful in preventing the deck from cracking and maintained small service deflections.

7. The accelerations of the girders were measured at the midspan during the dynamic portion of the truck load test. A 43.16 kips truck traveling in the left-hand lane at 65 mph demonstrated a vertical acceleration of 0.026g. The results from the other dynamic truck load tests were similar with respect to magnitude regardless of the

velocity of the truck. The maximum accelerations of faster moving trucks were no higher than those at lower speeds. The girder on which the maximum acceleration was recorded varied depending on the velocity of the truck. From the dynamic tests performed during this project, there is little correlation between velocity of the test load and maximum accelerations at midspan; however, the sample size was small. Given the nature of the accelerometer data, it is difficult to hypothesize on potential trends, and more data are needed before a firm conclusion can be drawn.

8. The cost of the GFRP deck was compared to a similar steel RC deck built at approximately the same time. The cost comparison on a per year basis was determined to be $1.10/sq. ft./yr for the GFRP deck and $1.09/sq. ft./yr of the steel deck. Further investigation into the lifespan of GFRP decks was made and resulted in an increase in the design life and corresponding decrease in cost on a per year basis. Changing the design life to 100 years provides a per-year cost of $0.66 /sq. ft/yr. The extended design life of the GFRP deck provided a monetary advantage over traditional steel RC decks, despite its higher initial capital cost.

REFERENCES

1. American Association of State Highway and Transportation Officials (AASHTO). (2009). *LRFD Bridge Design Specifications*, 4th Ed., AASHTO, Washington, D.C.

2. American Concrete Institute(ACI). (2006). *Guide for the Design and Construction of Structural Concrete Reinforced with FRP Bars, ACI 440.1R-06*, American Concrete Institute, Farmington Hills, MI.

3. Benmokrane, B., El-Salakaway, E., and Lackey, T. (2006). "Designing and testing of concrete bridge decks reinforced with glass FRP Bars." *Journal of Bridge Engineers*, ASCE, 11(2), 217-229.

4. Camisa, S., Tikalsky, P., and Schokker, A. (2003). *Instrumentation and Monitoring of HPC Bridge Decks*. The Pennsylvania Transportation Institute, State College, PA.

5. Deitz, D. H., Harik, I. E., and Gesund, H. (2003). "Physical properties of glass fiber reinforced polymer rebars in compression." *Journal of Composites for Construction*, ASCE, 7 (4), 363.

6. Eitel, A. (2005). "Performance of a GFRP Reinforced Concrete Bridge Deck" dissertation, presented to Case Western Reserve University at Cleveland, OH, in partial fulfillment of the requirements for the degree of Doctor of Philosophy.

7. Martin, L., and Perry, C. (2004). *PCI design handbook: precast and prestressed concrete*, 6th Ed., Prestressed Concrete Inst, Chicago, IL.

8. Mufti, A.A., Onofrei, M., Benmokrane, B., Banthia, N., Boulfiza, M., Newhook, J.P., Bakht, B., Tadros, G.S., and Brett, P. (2007) "Field study of glass-fibre-reinforced polymer durability in concrete." *Canadian Journal of Civil Engineering*, 34, 355-366.

9. Russell, H. (1996). "Guidelines for Instrumentation of Bridges" Report FHWA-SA-96-075, *U.S. Dept. of Transportation*, Washington, D.C.

10. Tang**,** B., (1997). “Fiber Reinforced Polymer Composites Applications in USA,“ *Department of Trasnportation-Federal Highway Administration*, <http://www.fhwa.dot.gov/bridge/frp/frp197.cfm > (October 5 2010).

11. Weber, A., and Baquero, C. W., (2010). “New Durability Concept for FRP Reinforcing Bars.” *Concrete International*, 32(7).